UNIVERSITY OF OKLAHOMA

GRADUATE COLLEGE

Design and development of a Selective Laser Sintering (SLS) 3D printer for potential biomedical engineering applications.

A THESIS

SUBMITTED TO THE GRADUATE FACULTY

in partial fulfillment of the requirements for the

Degree of

MASTER OF SCIENCE

By

John Jacob Hering

Norman, Oklahoma

2023

Downloaded from SHAREOK. Persistent Handle URL: https://hdl.handle.net/11244/337576

Design and development of a Selective Laser Sintering (SLS) 3D printer for potential biomedical engineering applications.

A THESIS APPROVED FOR THE SCHOOL OF AEROSPACE AND MECHANICAL ENGINEERING

BY THE COMMITTEE CONSISTING OF

Dr. Yingtao Liu, Chair

Dr. Jivtesh Garg, Co-Chair

Dr. Hanping Ding

© Copyright by John Jacob Hering, 2023

All Rights Reserved.

Acknowledgments

I would first like to thank Dr. Yingtao Liu at the University of Oklahoma for the opportunity to research in his lab for the past three years. Enriching my engineering education further under his guidance has been a privilege. I am also thankful to Dr. Blake Herron for introducing me to Dr. Liu and encouraging me to start undergraduate research. I would not be here today without his inspiration. In addition, I would like to thank Chris Billings for his insight and recommendations through occasional update meetings. I would also like to thank Elijah in the machine shop for ensuring all my parts were correctly manufactured. I am also grateful for the friendship and guidance from other graduate students within the additive manufacturing lab. Also, I would like to thank Dr. Jivtesh Garg for taking the time to aid in my graduate studies, as well as both he and Dr. Hanping Ding for taking an interest in my research as a member of my thesis committee.

I have met many outstanding students in undergraduate and graduate school. In the AME department, I am incredibly thankful for Will Gray and Lane Taylor, my closest friends with whom I shared many classes. I am also grateful for my roommates, Jack Lanza and Rylan McConaughey, who have always pushed and encouraged me. Lastly, I am forever thankful for the endless love and support my closest friends and family have provided.

Dedication Page

I want to dedicate this thesis to my late father, John Carroll Hering, who gave me endless love and support. He inspires me daily, and I know he would be so proud of all I have accomplished. I would also like to dedicate this thesis to my mother, sister, and fiancé, who have been my biggest supporters for the past year. I would not be here today without their love and encouragement.

Table of Contents

ACKNOWLEDGMENTS ..... **IV**

DEDICATION PAGE ..... **V**

TABLE OF FIGURES ..... **VII**

TABLE OF TABLES ..... **X**

ABSTRACT ..... **XI**

CHAPTER 1: INTRODUCTION **1**

SECTION 1.1: STATE OF THE ART OF 3D PRINTING IN THE BIOMEDICAL FIELD 1
SECTION 1.2: INKJET-BASED BIOPRINTING 3
SECTION 1.3: LASER-ASSISTED BIOPRINTING 4
SECTION 1.4: EXTRUSION-BASED BIOPRINTING 5
SECTION 1.5: STEREOLITHOGRAPHY-BASED-BIOPRINTING 6
SECTION 1.6: COMPARISON OF TECHNIQUES 7
SECTION 1.7: THESIS OUTLINE 8

CHAPTER 2: DESIGN AND OPTIMIZATION OF SLS PRINTER **9**

SECTION 2.1: INTRODUCTION 9
SECTION 2.2 MECHANICAL DESIGN 11
SECTION 2.3 ELECTRICAL COMPONENTS 22
SECTION 2.4 SOFTWARE CONFIGURATION 28
SECTION 2.5 PRINTER OPTIMIZATION 35

CHAPTER 3: 3D PRINTING OF SUGAR SAMPLES **37**

SECTION 3.1: SAMPLE MODELING AND G-CODE GENERATION 37
SECTION 3.2: PRINTING PARAMETERS 40
SECTION 3.3 SIMPLE SINGLE-LAYER SAMPLES 42
SECTION 3.4: COMPLEX SINGLE-LAYER SAMPLES 44

CHAPTER 4: MEASUREMENT AND GEOMETRY SHAPE VALIDATION **46**

SECTION 4.1: SAMPLE MEASUREMENTS 46
SECTION 4.2: DENSITY TEST 50
SECTION 4.3: GEOMETRY SHAPE VALIDATION 53

CHAPTER 5: CONCLUSION AND FUTURE WORK **55**

REFERENCES **57**

Table of Figures

Figure 1: Most Common 3D Printing Methods for Bioinks [7] 2

Figure 2: Inkjet-Based Bioprinting Diagram [11] 3

Figure 3: Laser-Assisted Bioprinting Diagram [13] 4

Figure 4: Extrusion-Based-Bioprinting Diagram [16] 5

Figure 5: Stereolithography-Based-Bioprinting Diagram [19] 6

Figure 6: Manufacturing Piezoelectric Sensors for Biomedical Applications [23, 24] 9

Figure 7: Selective Laser Sintering (SLS) Printing Process [26] 10

Figure 8: Piston Housing Manufactured out of T6061 Aluminum 11

Figure 9: Piston Housing Installed in Printer 12

Figure 10: Assembled Internal Piston 13

Figure 11: Movement of the Delivery and Fabrication Piston 14

Figure 12: Sweeper Arm for Sugar Deposition 15

Figure 13: The Heat Chamber 16

Figure 14: Heat Chamber Insulation 16

Figure 15: Heat Chamber Glass Viewing Windows 17

Figure 16: X and Y Dimensional Laser Control 18

Figure 17: Core XY Belt System Diagram 18

Figure 18: NEMA Stepper Motor 19

Figure 19: Homing X and Y Axis Using Limit Switches 20

Figure 20: Homing Piston and Sweeper Arm Axis Using Limit Switches 21

Figure 21: Duet 3D Mini 5+ Wi-Fi Board 22

Figure 22: Temperature Controller and Heat Sink Solid State Relay 23

Figure 23: SolidWorks Rendering of Heating Element 24

Figure 24: Heating Elements Installed in the Heat Chamber 25

Figure 25: Heat Bed Validation 26
Figure 26: Aluminum Alloy 4W Laser Engraver 26
Figure 27: 24V to 12V Buck converter 27
Figure 28: Custom Duet Configuration File Code 29
Figure 29: Duet Configuration File Laser Code 30
Figure 30: Diagram of the Steps in the Printing Process 31
Figure 31: Layer Change Pseudocode 32
Figure 32: Adjusting Laser Intensity 33
Figure 33: Laser Activation Command Replacement Code 33
Figure 34: Controlling Printer Movement in Duet Interface 34
Figure 35: Pure Cane Sugar 35
Figure 36: Slanted Laser Position 36
Figure 37: Square Sample Generation 37
Figure 38: Density Test Sample Generation 37
Figure 39: Star Sample Generation 38
Figure 40: Leaf Sample Generation 38
Figure 41: Bird Sample Generation 39
Figure 42: Square Samples 42
Figure 43: Density Test Samples 43
Figure 44: Star Sample 44
Figure 45: Leaf Sample 44
Figure 46: Bird Sample 45
Figure 47: Chart of Simple Single-Layer Samples 46
Figure 48: Area of Simple Single-Layer Samples 47
Figure 49: Chart of Complex Geometry Single-Layer Samples 48

Figure 50: AccuPyc II 1340 Gas Pycnometer to Measure the Density Test Samples 50
Figure 51: Average Density of Three Density Test Samples 51
Figure 52: OptixCam Summit K2 Camera attached to Omano Microscope 53
Figure 53: Close-up of the Sintered Sugar in a Square Sample..... 53
Figure 54: Close-up of the Sintered Sugar in a Density Test Sample 54

Table of Tables

Table 1: Comparison of 3D Bioprinting Techniques [21] 7

Table 2: Marlin G-Code Command Library 28

Table 3: Core-XY Coordinate Movement Based on Motor Rotation 31

Table 4: Printing Parameters for Square Samples 40

Table 5: Printing Parameters for Density Test Samples 41

Table 6: Printing Parameters for Star Samples 41

Table 7: Printing Parameters for Leaf Samples 41

Table 8: Printing Parameters for Bird Samples 41

Table 9: Mass of Single Layer Samples 46

Table 10: Area of Simple Single-Layer Samples 47

Table 11: Mass of Complex Geometry Samples 48

Table 12: Density Test Sample Volume 51

Table 13: Density Test Sample Density 51

Abstract

An additive manufacturing method called Selective Laser Sintering (SLS) involves heating material particles to bond them together. Each two-dimensional layer is selectively sintered in the fabrication piston until the part is entirely manufactured. New layers are created by depositing material from the delivery piston to the fabrication piston, where the laser will follow the cross-sectional toolpath generated from a slicer. One of the most significant advantages of SLS 3D printing is that there is no need to have structural support for the material. The unused material provides support for the sintered shape throughout the whole process. Due to its biocompatibility and mechanical properties, sugar can be a biodegradable structure with many applications in biomedical engineering, such as sugar skeletons for tissue engineering and drug delivery [1]. Thus, this thesis examines the SLS process to print simple and complex geometry single-layer sugar samples. Each sample is designed to showcase the sintering capabilities and technology of an SLS 3D printer for potential biomedical engineering applications. Each sample is sliced into its cross-sectional layers using a non-proprietary software called Slic3r; its G-Code is translated to generate the lasers toolpath, then uploaded to the printer. The printing parameters such as heat chamber temperature, laser scanning speed, and laser intensity are the major determining factors in sample accuracy. Therefore, ideal printing parameters are discussed, and samples are evaluated through various tests. Results show that this printer can sinter single-layer sugar samples in multiple geometries to an acceptable level of accuracy. The printer is limited to two-dimensional printing. However, the results of the final samples indicate that this printer will be able to print in three dimensions in future research.

Chapter 1: Introduction

Section 1.1: State of the art of 3D printing in the biomedical field

3D printing is part of a process known as additive manufacturing (AM), where an object is created by adding material in a layer-by-layer method. It differs from traditional manufacturing methods, which typically involve shaping and assembling pre-existing materials. Additive manufacturing allows for building complex shapes and geometries that would be difficult or impossible to produce using traditional methods. It also allows for creating customized products, as the digital file can be easily modified to make changes to the design. In recent years, additive manufacturing has become increasingly popular and used in various industries, including aerospace, automotive, and biomedical [2-11].

Additive manufacturing has the potential to revolutionize the biomedical field by providing a way to create customized medical devices and implants. For example, 3D printing can create prosthetics tailored to a patient's body's exact shape and size. Tailored fits can lead to a more comfortable and functional prosthetic and a faster and more straightforward fitting process [12]. In addition to prosthetics, 3D printing can create tissue and organ structures for drug testing or transplantation [13]. While this is still an area of active research, it has the potential to improve the treatment of diseases and injuries significantly. Additively manufactured products can also be used to improve public health due to their antimicrobial capabilities [14-16].

Bioinks are materials used in some biomedical 3D printing applications to create structures that mimic the complexity of natural tissues. Bioinks are made from cells, extracellular matrix (ECM) proteins, and other biomolecules that can support the growth and function of living cells [17]. Bioinks can create 3D-printed structures similar in composition and structure to neural, cardiac, cartilage, vasculature, bone, and skin tissues [18]. From their ability to promote

cell attachment and differentiation, bioinks can revolutionize how we treat illnesses and injuries, drug testing, cancer research, and disease modeling [19].

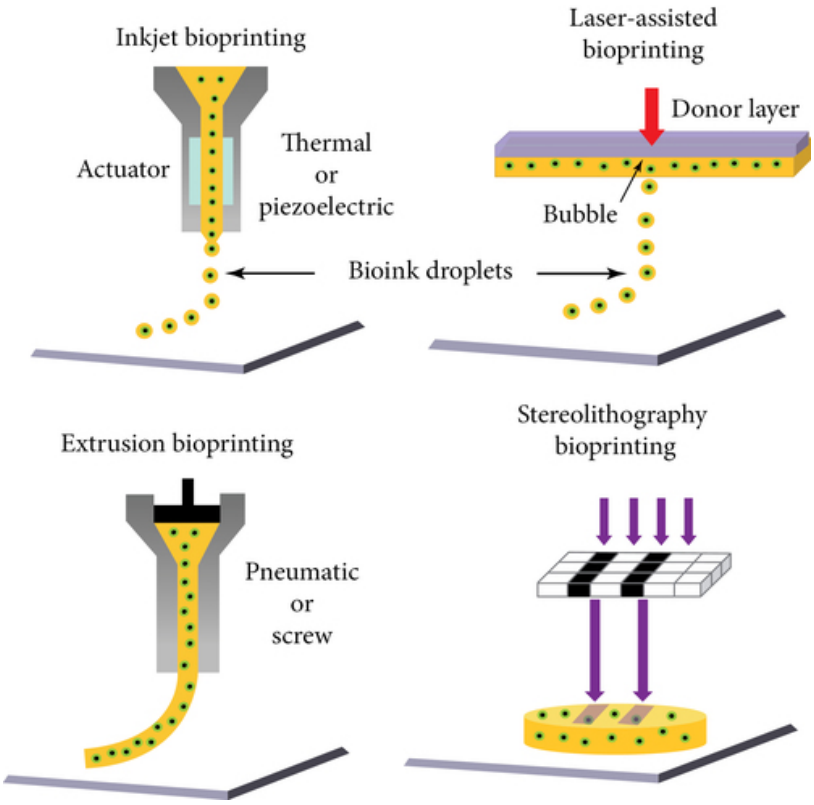


Figure 1: Most Common 3D Printing Methods for Bioinks [20]

The most popular additive manufacturing methods for bioinks are inkjet-based-bioprinting, laser-assisted-bioprinting, extrusion-based-bioprinting, and stereolithography bioprinting [21]. As printing techniques have reached increasing levels of precision, they have evolved the ability to produce hyper-realistic models of complex organs [22]. This technology is eventually expected to solve the lack of organ donors for people waiting for critical organs such as hearts, kidneys, and livers [23]. Though much work remains, 3D printing offers a promising future for biomedicine.

Section 1.2: Inkjet-based bioprinting

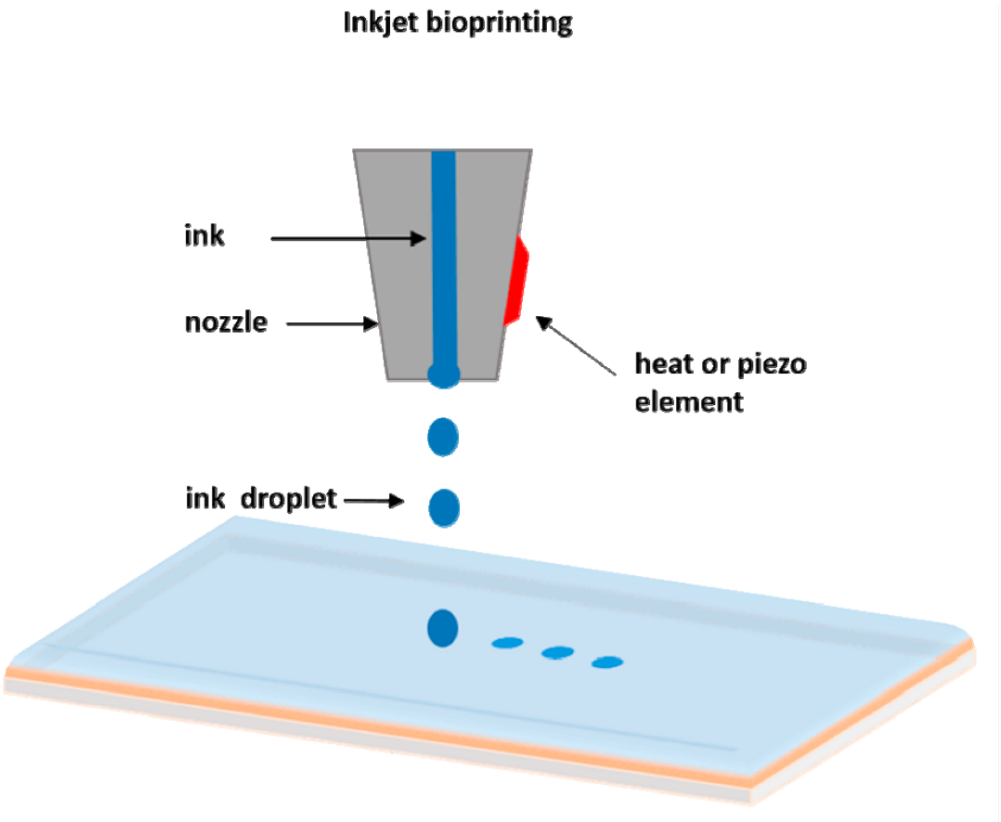


Figure 2: Inkjet-Based Bioprinting Diagram [24]

Inkjet-based bioprinting is a method of 3D printing that uses an inkjet printer to deposit biological materials, such as cells, onto a substrate to create living tissue [25]. The bioink droplets are printed in a pattern based on a digital file to create the desired 3D structure. This technology is still in its early stages of development. Still, it has the potential to be used for a variety of applications. Some potential applications include creating 3D models of tumors for cancer research, producing functional blood vessels for tissue engineering, and developing 3D cell cultures for drug testing [25].

Section 1.3: Laser-assisted bioprinting

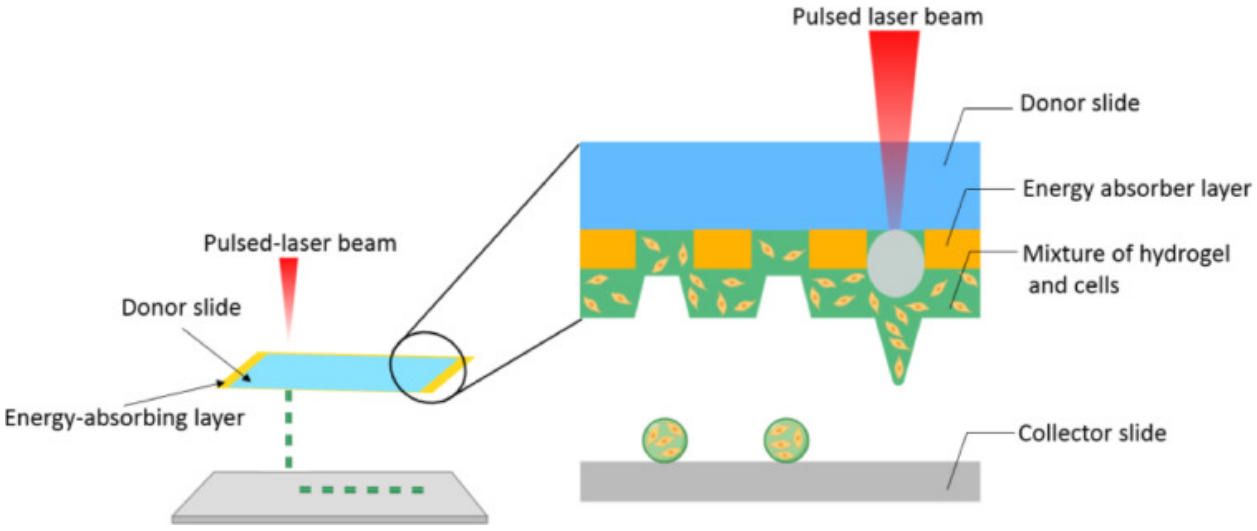


Figure 3: Laser-Assisted Bioprinting Diagram [26]

Laser-assisted bioprinting is a technology that utilizes a laser to precisely manipulate biological materials, such as biomaterials, to create 3D structures [27]. The laser beam cuts, shapes, or sinters biological materials to build complex 3D structures. This is like the technology this thesis explores, as a laser will sinter sugar, a biocompatible material. Examples of laser-assisted bioprinting include creating 3D structures of bones, cartilage, and skin for regenerative medicine, creating functional vasculature for tissue engineering, and sintering sugar skeletons for tissue engineering [28]. In addition, laser-assisted bioprinting can be used to create structures with a high level of detail and accuracy, which is vital for many medical applications.

Section 1.4: Extrusion-based bioprinting

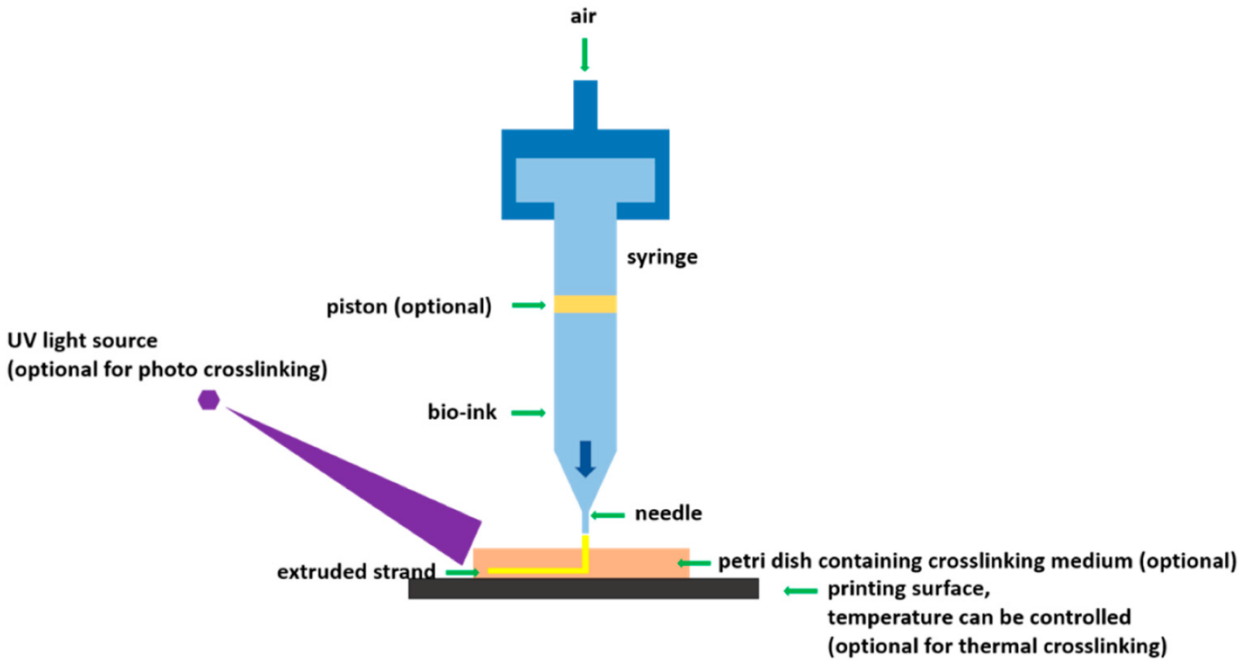


Figure 4: Extrusion-Based-Bioprinting Diagram [29]

Extrusion-based bioprinting is a technology that uses a nozzle to extrude biological materials, such as cells and biomaterials, to create 3D structures [30]. The nozzle deposits the biological materials precisely, layer by layer, to build complex 3D structures. This technology is like traditional 3D printing but uses biological materials instead of plastics or metals. The advantage of extrusion-based bioprinting is creating highly complex structures relatively inexpensively and straightforwardly [30]. It is often used in biomedical research to develop organoids, miniature versions of organs that can be used for research and drug development [31]. Despite being used mainly in research exposure, extrusion-based bioprinting can be used in various biomedical applications.

Section 1.5: Stereolithography-based-bioprinting

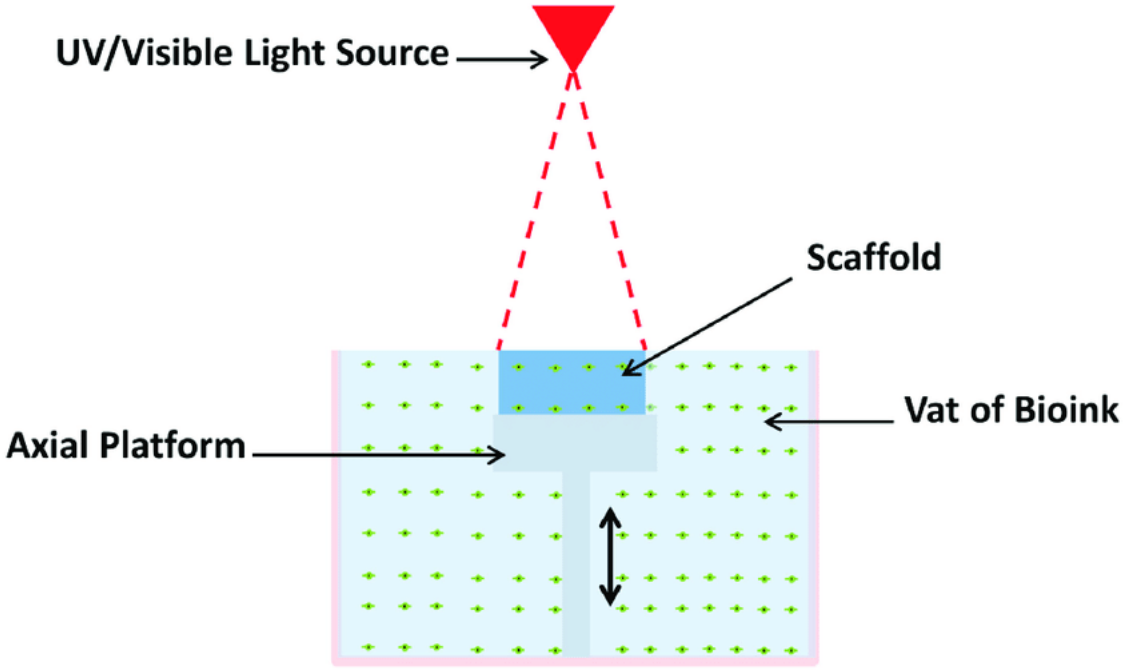


Figure 5: Stereolithography-Based-Bioprinting Diagram [32]

Stereolithography (SLA) is a 3D printing technology that uses a laser to cure layers of a photopolymer resin, one layer at a time, to build a 3D object. It is one of the oldest forms of 3D printing, commonly used to produce high-quality, accurate parts with a smooth surface finish [32]. SLA is one of the technologies that can be used for bioprinting, as it allows for precise control of the shape and size of the printed tissue [32]. However, there are many challenges to overcome before bioprinting becomes a widespread clinical reality, including developing more robust materials that can be printed by SLA and developing techniques to vascularize the printed tissue to receive the necessary nutrients and oxygen [33].

Section 1.6: Comparison of Techniques

Inkjet-based bioprinting uses traditional inkjet printing, where tiny droplets of material are precisely deposited to create 3D structures. Laser-assisted bioprinting uses a laser to bond material and create 3D structures. Extrusion-based bioprinting uses a nozzle to extrude material, building up layers to create 3D structures. Stereolithography-based bioprinting uses a laser to solidify a liquid photopolymer, building layers to create 3D structures. The differences between all types of 3D bioprinting techniques are outlined in Table 1 below.

Table 1: Comparison of 3D Bioprinting Techniques [34]

Properties	Inkjet-based	Laser-assisted	Extrusion-based	Stereolithography-based
Ink viscosity	3.5-12 mPa/s	Up to 6 x 10^7 mPa/s	1-300 mPa/s	No limitation
Cell density	Low, <10^6 cells/ml	No limitation	Medium, <10^8 cells/ml	No limitation
Resolution	High	Moderate	High	High
Print speed	Fast	Slow	Medium	Fast
Cost	Low	Medium	High	Low

Some notable differences in Table 1 are that inkjet-based and extrusion-based bioprinting have the highest print resolution compared to the other techniques. Inkjet-based and stereolithography-based have the fastest print speed and the lowest cost. All these methods have advantages and disadvantages, such as resolution and printing speed, and are suitable for different applications. The best technology would depend on the desired outcome, budget, and other factors.

Section 1.7: Thesis outline

This thesis examines the design and development of an SLS 3D printer, sintered sugar samples, and potential biomedical applications. The thesis is divided into five chapters highlighting the printer's capabilities. In Chapter 2, the origin of the printer and its basic functionality are discussed. The mechanical and electrical components and their functions are explored, such as the printer's structure, mechanisms, software, and techniques used to optimize the printer. In Chapter 3, sample prints of the SLS printer are demonstrated. This chapter reviews the printing process from G-Code generation, printing parameters, and samples of various complexity. These samples are intended to highlight the printer's potential. Chapter 4 tests the samples to determine the mass, density, surface smoothness, and flatness profile. Lastly, Chapter 5 will discuss the conclusions and future work.

Chapter 2: Design and Optimization of SLS Printer

Section 2.1: Introduction

SLS 3D printing in the Smart Materials and Intelligent Systems (SMIS) Laboratory at the University of Oklahoma began in 2018. This area of research was established by Benjamin Hoelzel, a graduate student, who created an SLS printer to print a thermoplastic called High-Density Polyethylene (HDPE) for his master's thesis. The selective laser sintering printer used for his thesis was constructed and modeled after the Johannes Rostek Laser Sintering 1000 (JRLS), an SLS printer developed by German engineer Johannes Rostek. This SLS printer was chosen to be modeled mainly because its design included a heat chamber that would allow the HDPE samples to be printed without curling or warping [35]. The need for a larger SLS 3D printer began after Dr. Yingtao Liu published research papers where piezoelectric sensing devices were created by injecting electrically conductive nanocomposites into sacrificial sugar skeletons [9]. His research, which combines nanocomposites and sugar skeletons, focuses on producing wearable sensory technology that provides aid to rehabilitation patients [9]. The SLS printer in this thesis was developed to continue using sugar for biomedical applications and explore other possibilities of SLS technology. Figure 6 below shows the production process for Dr. Liu's research using sourced, generic sugar cubes.

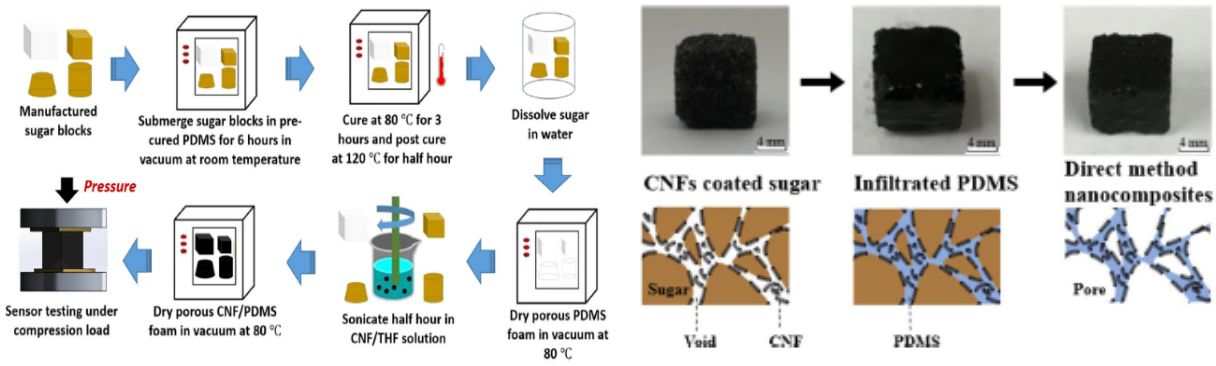


Figure 6: Manufacturing Piezoelectric Sensors for Biomedical Applications [9, 36]

Selective laser sintering (SLS) is a type of 3D printing that uses a laser to sinter layers of powdered material to create a 3D object. SLS 3D printers typically consist of a fabrication piston, a laser, and a powder delivery piston with a mechanism to move material evenly [37]. The fabrication piston is generally heated to a temperature just below the melting point of the powdered material [37]. The laser is used to selectively sinter the powdered material in a predetermined pattern based on a digital file. As the layers of powdered material are fused, the fabrication piston is lowered, and more powdered material is added. This process is repeated until the entire object has been printed, as shown in Figure 7 below.

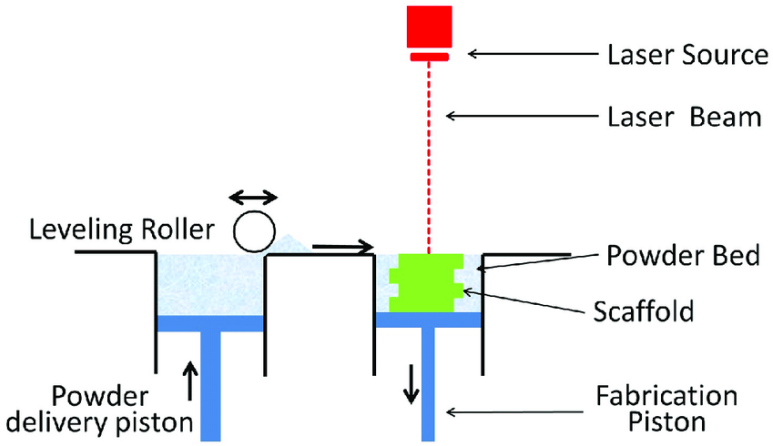


Figure 7: Selective Laser Sintering (SLS) Printing Process [38]

This printer harnesses the SLS technology to reduce the porous spaces between the sugar particles and bond the loose sugar into a solid sample. Just as a material has a melting point, it will also have a desirable sintering point. A study on Sucrose Powder in an SLS Printer determined that the melting point of sugar was just under 187℃ [39]. Therefore, sintering was assumed to occur around 180℃, just below the melting point. When printing samples, the heat chamber temperature is set to around 160℃, and the laser heats the sugar enough to the sintering temperature to bond the sugar.

Section 2.2 Mechanical Design

The piston housing is centrally located and is machined from ½-inch 6061 aluminum sheets at the University Machine shop. There are three vertical aluminum plates and four horizontal running plates. The vertical plates connect to the external 2020 square aluminum tubing and are the foundation of the printer's support structure. The horizontal plates further separate the sections where the piston operates; therefore, the housing requires accurate construction. The parts were machined using a Summit 3-axis mill, band saw, drill press, and other equipment. Eight external screw holes were tapped to fasten the horizontal plates using an M6x1.0 thread tap. All other threaded holes were tapped using an M5x0.8 thread tap to connect to 202 square tubing. The center plate has four 5mm smooth steel rods pressed for the horizontal plates to attach. Each horizontal plate is further supported by two set screws facing the outsides.



Figure 8: Piston Housing Manufactured out of T6061 Aluminum

The piston housing is shown in Figure 8 above and is responsible for supporting and separating the heating chamber, piston assembly, gantry system, and other electronics. It acts as the reinforcing backbone of the entire printer.

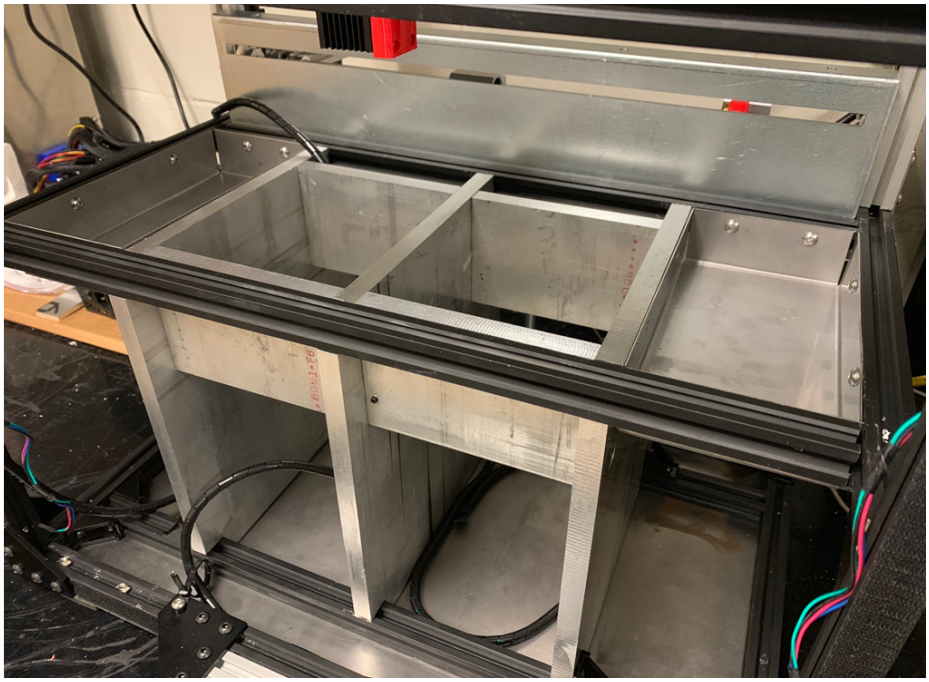


Figure 9: Piston Housing Installed in Printer

As shown in Figure 9, the piston housing sits in the center part of the printer. Then the frame of the printer was assembled from 2020 aluminum extrusion, T-nuts, and M4 bolts. This created the necessary structure, allowing the rest of the mechanical parts to be added. The center two cutouts are for the two pistons. The piston on the left is the powder delivery piston, where the sugar is stored, and the piston on the right is the fabrication piston, where the sugar is sintered. Top plates are added to the pistons to hold the sugar in place. It is essential to have an adequately manufactured frame to seal the pistons appropriately. This ensures that sugar is maintained within the piston while minimizing the heat leaked from the printing area. These pistons are an essential part of an SLS printer and are considered the Z-axis of the printer.



Figure 10: Assembled Internal Piston

The assembled internal piston shown in Figure 10 above was created from three different materials. The top and bottom plates, known as the powder and lift plate, were manufactured from ½-inch thick aluminum in the AME machine ship. The wood block is 3.5x3.5x4 inches and is made from solid birch wood. Then, calcium silicate was attached on both sides of the wood block to insulate the internal pistons. Both are light materials that help control the Z-axis motors connected to the pistons easier. Wood is also a rigid, moisture-resistant material with very low thermal conductivity. For these reasons, it was selected to elevate the top plate of the fabrication piston while controlling the heat flux to the print layer. The wood block sets in a recessed cavity in the lift table for each piston. These lift tables have been laser cut from ¼ in 6061 aluminum. The lift tables attach to 12mm rails on the Z-axis by attaching a linear bearing seen in Figure 11 below.

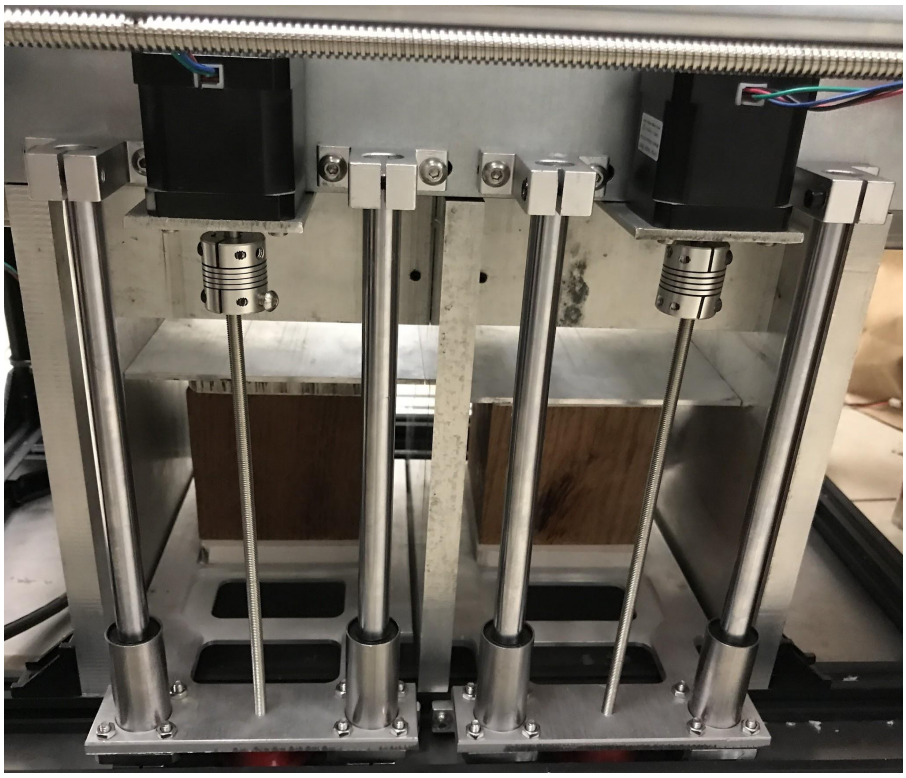


Figure 11: Movement of the Delivery and Fabrication Piston

The pistons lift plates are placed through 5mm threaded rods attached to NEMA stepper motors shown in Figure 11. The 12mm rails were inserted through the slide ball bearings, which guide vertical piston movement. The 5mm threaded rod in the center of the lift plate is fastened from the upper rod coupling connected to the motors to a lower 5mm ball bearing. Both pistons have the same assembly. Once the lift plates are attached, the stepper motors can control the vertical travel of the lift plates by rotating the 5mm threaded rod through the plates. The two pistons are programmed to counter-rotate, which means when the fabrication piston is elevated, the powder delivery piston descends and vise-versa. The programming of the pistons is discussed in more detail in Section 2.3.



Figure 12: Sweeper Arm for Sugar Deposition

The sweeper arm is part of the printer that pushes sugar from the delivery piston to the fabrication piston. The arm must have level contact with the heating chamber's bed and consistent sugar deposition onto the fabrication piston. A wooden dowel was chosen because it has a high melting temperature and is easy and cheap to create. It may be necessary to replace this part with metal if the wood begins to warp with time or temperature. The wooden dowel is attached to the metal arm with super cyanoacrylate glue. Cyanoacrylate breaks down at around 600° Celsius, much higher than temperatures in the heat chamber. Springs were also added to the sweeper's arm as an adjustable spacer to set the height of the wooden dowel over the bed. Future research on this printer will be able to use the total capacity of the sweeper's arm when 3D printing is attempted. For this thesis, only 2D printing is considered because the sweeper arm does not deposit enough sugar onto the fabrication piston. This is the essential printer feature when printing in three dimensions because it deposits new layers. This feature will unlock one of the most valuable benefits of SLS printing, allowing excess powder not sintered to support the print. Dr. Liu can then print complex sugar skeletons without manually printing support structures necessary in other 3D printing techniques, such as extrusion-based FDM 3D printing.

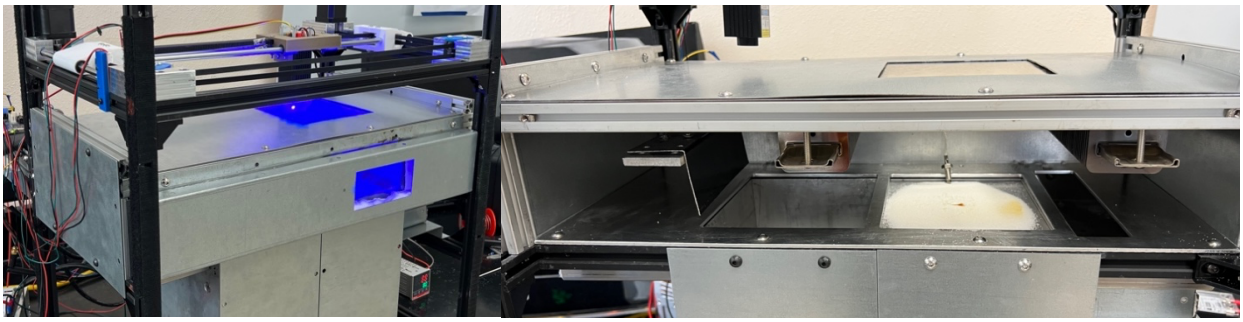


Figure 13: The Heat Chamber

A controlled environment, such as a heat chamber, is needed to achieve and maintain adequate temperatures during printing. It provides and maintains optimal temperatures for sintering the sugar and helps protect heat-sensitive components like the control board. The chamber was constructed with an internal layer of 18-gauge galvanized steel broken and punched on precision machinery. The inner steel sheets were fastened to the inside of the aluminum 30x30mm frame with 5x.08mm button head screws.

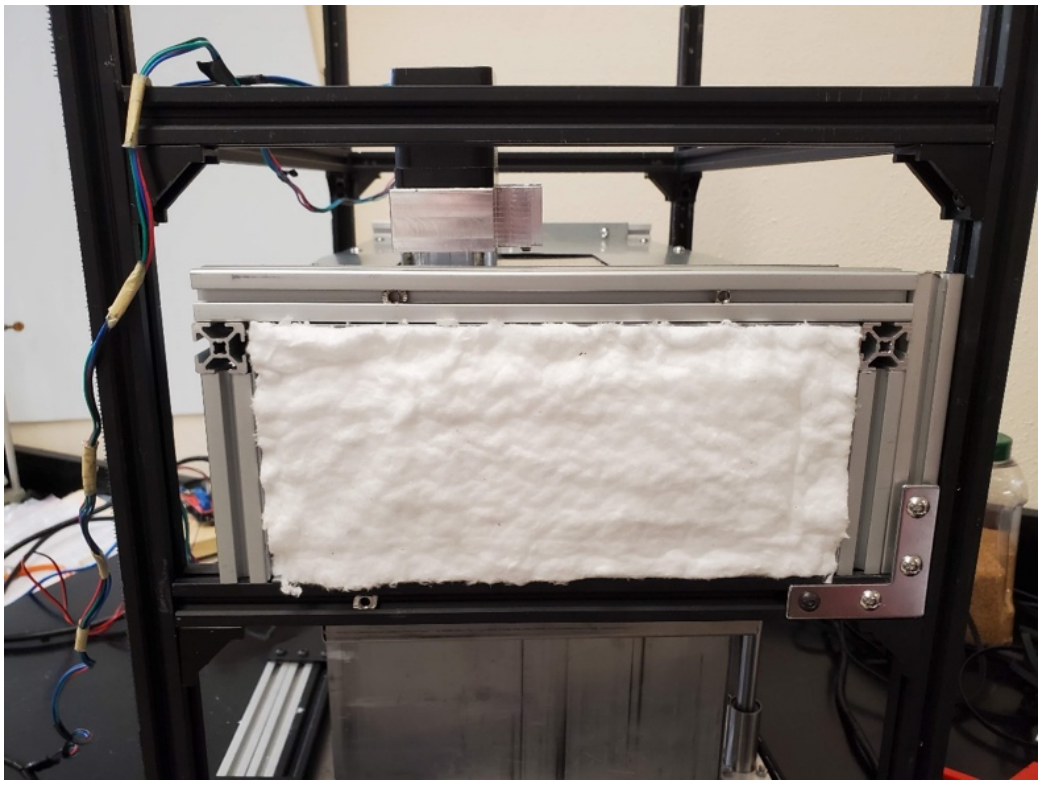


Figure 14: Heat Chamber Insulation

In between the first and second layers of the thermal panels, there is 1-inch-thick fiberglass insulation that was cut from a roll to fit tightly in the panel cavity, as seen in Figure 14 above. The second 18-gauge galvanized steel sheet is placed over the fiberglass insulation and is fastened to the outer 30x30mm aluminum frame with 6x0.8mm button head screws. The panels are designed to overlap to avoid heat conduction through the galvanized steel to the exterior. Since heat is known to travel through the path of least resistance, heat must be forced to travel through the insulation and not around it through the steel. The front panel is fastened using pop rivets on the top and bottom flanges. This separates the front thermal panel by removing only two screws on each side while maintaining a tight fit on the frame.



Figure 15: Heat Chamber Glass Viewing Windows

Finally, as seen in Figure 15, the chamber has two cutouts. One cutout is on the top, allowing the laser to sinter the sugar on the piston. The second cutout is in the front panel, which enables the operator to observe the print process. Each cutout is covered with ¼-inch ceramic glass rated well over 180° Celsius. Since this printer uses an intense pulse light laser, it is recommended to wear laser safety glasses to protect the eyes from the dangers of lasers.

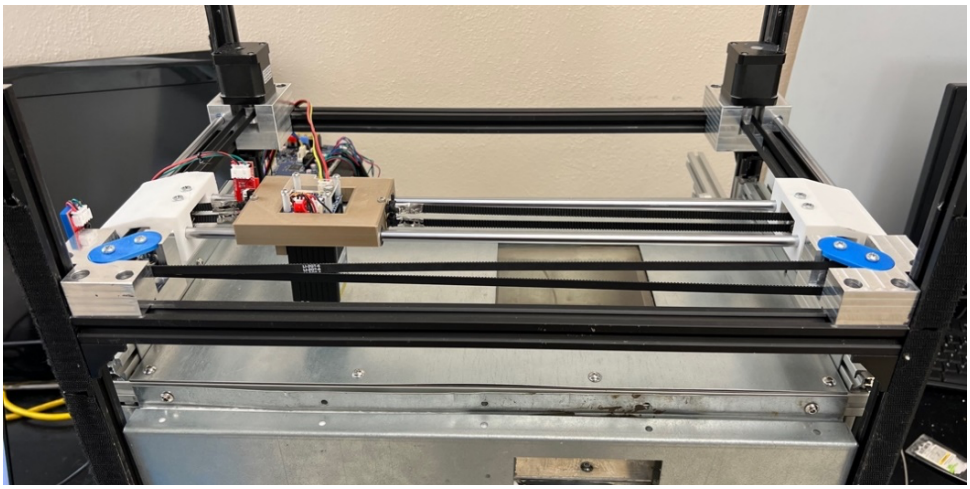


Figure 16: X and Y Dimensional Laser Control

To sinter material, the laser must move with precision and accuracy. This movement will be done by using a CoreXY 2-axis gantry system. The precision movements are done using two stepper motors located at the back corners of the printer's top. The picture in Figure 16 above shows the printer's gantry system configuration. Besides the two NEMA stepper motors, the gantry system includes two belts, four belt tighteners, the gantry that carries the laser, and other parts to support the movement of the belts.

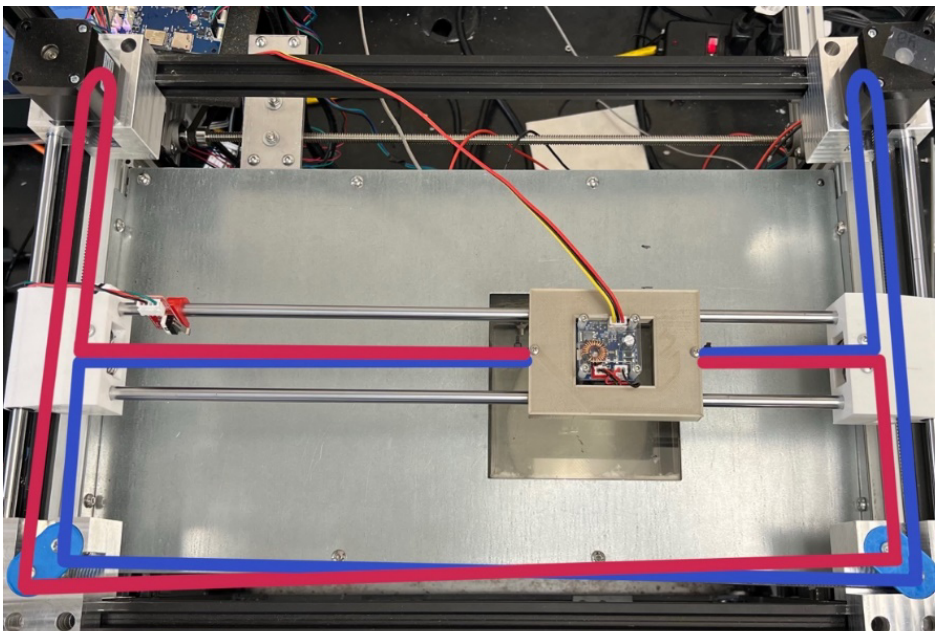


Figure 17: Core XY Belt System Diagram

A CoreXY belt system uses two perpendicular belts to drive the movement of the laser. As shown in Figure 17 above, the belt system has a top belt whose path is outlined in red and the bottom belt whose approach is outlined in blue. The main advantage of a CoreXY belt system is its ability to provide precise and accurate laser movement. This is because the two belts work together to create smooth and consistent motion, with the laser's movement determined by the two belts' relative tension. Another advantage of the CoreXY belt system is that it allows for faster printing speed as the print head can simultaneously move in both X and Y directions. Also, it can have a more stable structure, allowing for higher precision and accuracy.

As discussed further in Section 2.3, the gantry system moves diagonally instead of linear if only one motor rotates in a Core XY system. Both motors must turn in the same direction for linear motion in the X direction. Conversely, both motors must rotate in opposite directions to move in only the Y direction. To address this, software changes were necessary to account for this type of movement system.

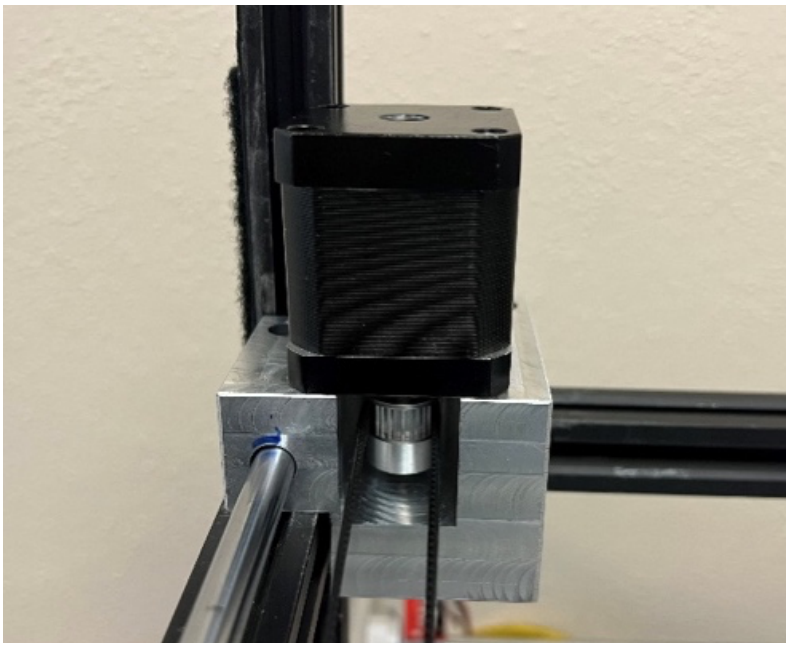


Figure 18: NEMA Stepper Motor

This printer utilizes five NEMA 17 motors, two in the gantry system, as shown in Figure 16. One in the sweeper arm system, as shown in Figure 12. And two in the piston system, as shown in Figure 11. They are named after the NEMA standard that defines the dimensions and mounting features of the motors. These stepper motors are electric motors that can be controlled to rotate in precise "steps" or increments rather than continuously. This makes them well-suited for applications requiring accurate and repeatable positioning. NEMA stepper motors are typically available in various sizes, with different frame sizes, step angles, and torque outputs. The NEMA 17 stepper motors with a step angle of 1.8 degrees rotate 1.8 degrees for each step. These motors were selected because they have several advantages over other motors. They are relatively simple to control and easily integrated into various applications. They have high torque at low speeds and do not require any feedback mechanism to determine the position of the rotor.

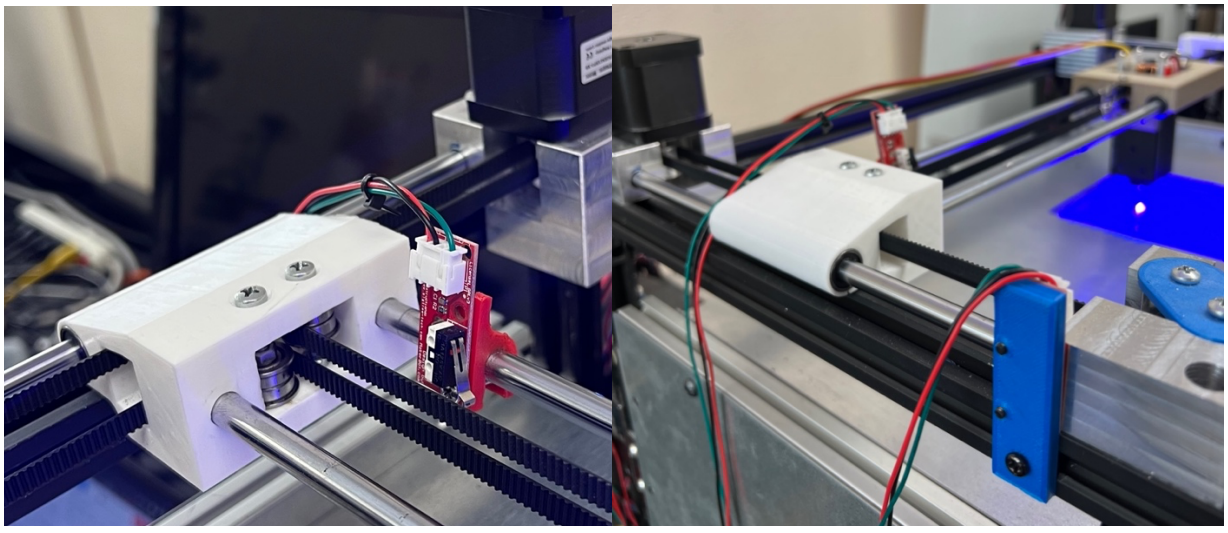


Figure 19: Homing X and Y Axis Using Limit Switches

Limit switches were installed in this printer to determine the physical limits of the printer's movement. They are installed at the end of the X, Y, Z (piston), and U (sweeper arm) axis shown in Figure 19 and Figure 20. These determine when the printer has reached the maximum or minimum position along that axis.

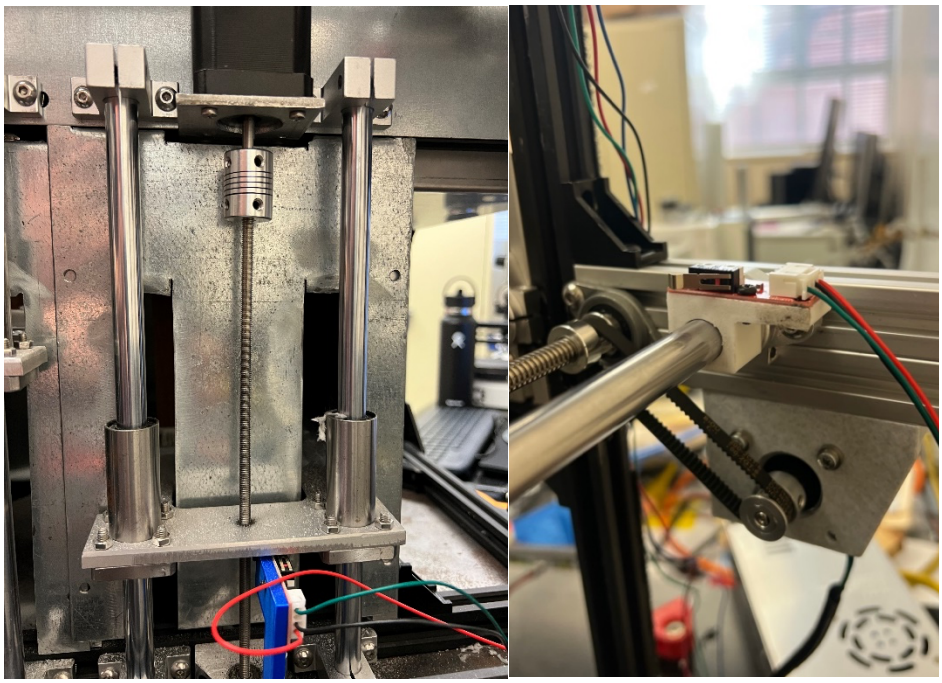


Figure 20: Homing Piston and Sweeper Arm Axis Using Limit Switches

When a limit switch is triggered, it sends a signal to the printer's control board, which stops the affected axis's movement. This helps to prevent the printer from crashing or damaging itself by moving beyond its physical limits. Limit switches also play an essential role in the calibration and homing process. During calibration, all 4 axes move toward a limit switch to determine the end and adjust their position accordingly. This allows the printer to accurately locate the home position of each axis, which is necessary for accurate printing. These limit switches are activated when the physical lever is pressed. Limit switches make the printer more robust and less prone to damage from unexpected movement.

Section 2.3 Electrical Components

In addition to the mechanical components discussed in Section 2.2, the printer possesses electrical components necessary to create samples. These electrical components include a Duet 3D Mini 5+ Wi-Fi Board, a temperature controller with a K sensor thermocouple, a heat sink solid state relay, two heaters, and a laser.

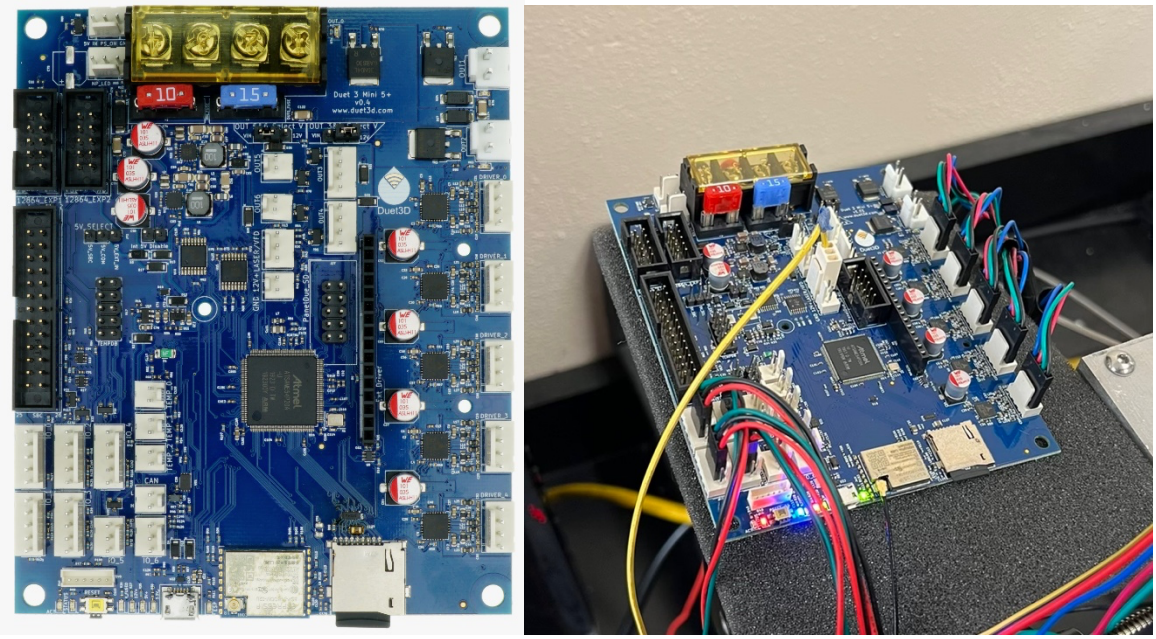


Figure 21: Duet 3D Mini 5+ Wi-Fi Board

The Duet 3D Mini 5+ Wi-Fi board shown in Figure 21 is a compact and powerful control board designed specifically for 3D printers. The board is powered by a 32-bit ARM processor, which ensures fast and smooth operation, even when running complex 3D prints. It also features four TMC2209 stepper drivers that support up to 2.4A RMS current and 256 micro-steps, precisely controlling the printer's motors. The board has expansion ports that allow for additional stepper drivers and a Pulse Width Modulation (PWM) port for the laser. The board runs on the latest version of the RepRapFirmware, a popular open-source firmware for 3D printers.

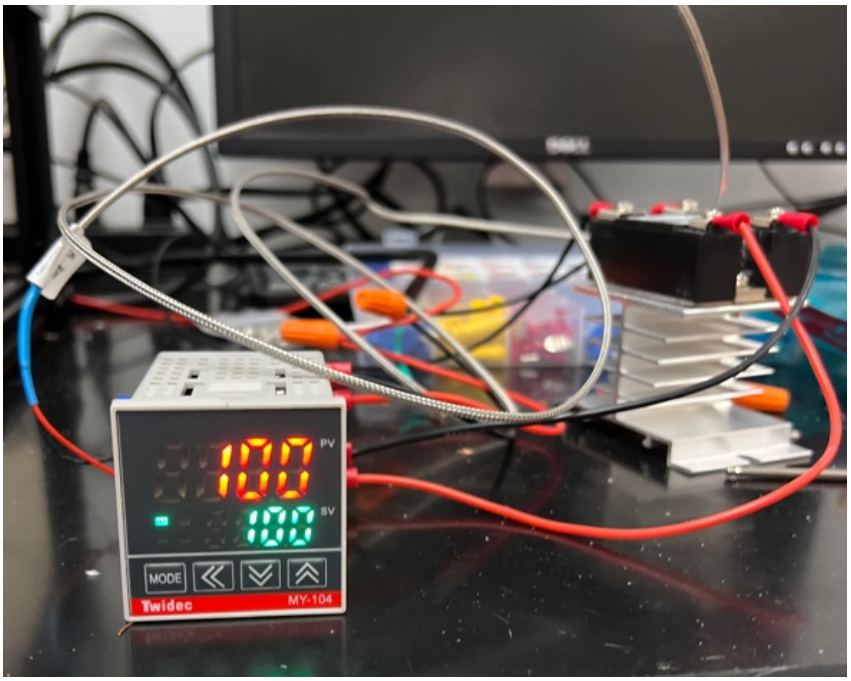


Figure 22: Temperature Controller and Heat Sink Solid State Relay

The temperature of the heat chamber varies based on the temperature controller, K sensor thermocouple, and solid-state heat sink relay. Once the temperature of the thermocouple reaches the set temperature in green, the solid-state relay will cut the circuit to turn the heaters off. The heater will provide convective heating throughout the heat chamber. Convection heating occurs when the thin layer of molecules in direct, physical contact with the heater heat up through the conduction process and causes them to expand. As they do, they move away from the heater, displacing the cooler, denser molecules in the chamber. They are forced to meet the heater, which warms them up, forcing them to expand and displace more air, which gets heated. This is what is known as a convection current. Because air is a poor heat conductor, convection heating works slowly, warming the air until it reaches the desired temperature. This heater uses a similar process to generate heat by running electricity through metal coils. The ceramic plates absorb the heat from the coils and warm up the surrounding air. The heating element used is shown in Figure 23 below.



Figure 23: SolidWorks Rendering of Heating Element

The heating elements in the heat chamber keep the temperature to around 160° Celsius. The heating elements are Finned Strip Heaters with inline screw terminals shown in Figure 23. Finned strip heaters convert electrical energy into heat, which is transferred to the surrounding environment via a finned metal strip. Finned strip heaters are typically used in applications that require a uniform distribution of heat over a large area, which is necessary for the heat chamber. In the heat chamber, these heating elements warm the sugar in the fabrication piston closer to its sintering temperature, around 180°C. The heaters are 725W and 120V, with a maximum heat output of 1200°C. The heating element is 10.5x2x1.375in and has a part number of 3575K424 from McMaster-Carr.

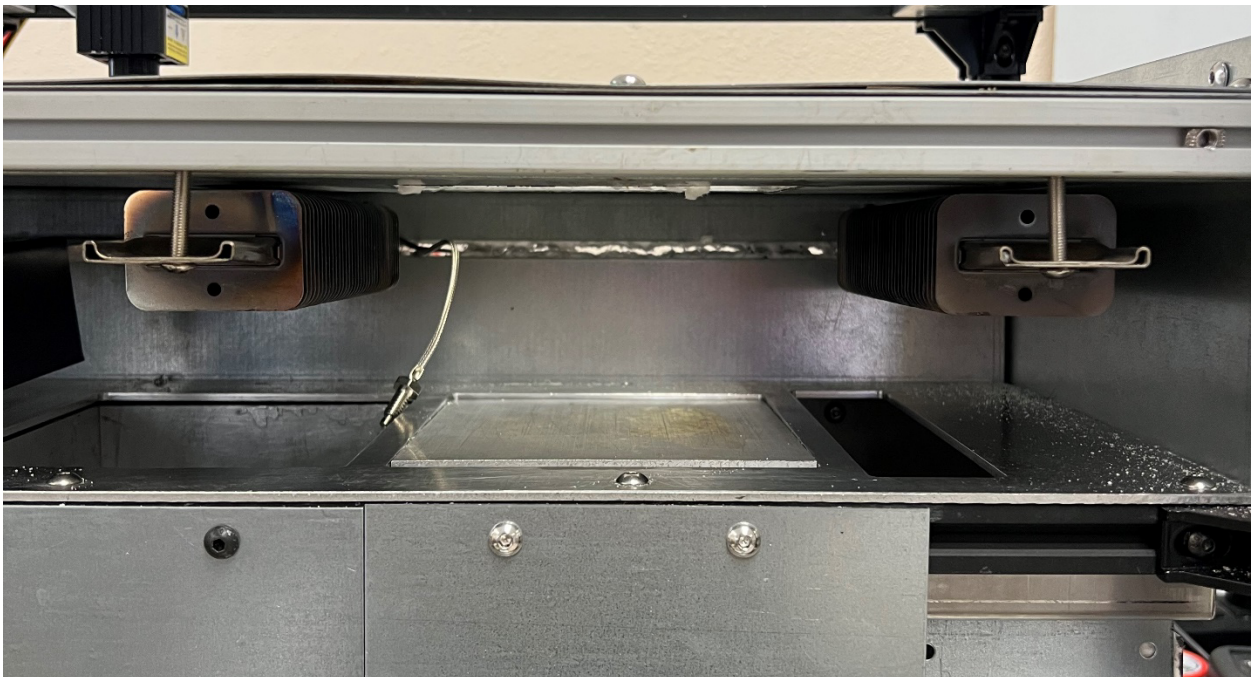


Figure 24: Heating Elements Installed in the Heat Chamber

The heating elements are installed onto the chamber's top and on either side of the fabrication piston. In addition, the thermocouple connected to the temperature controller in Figure 22 above is placed onto the fabrication piston to deactivate the relay when the desired temperature is reached. In SLS 3D printing, evenly distributed heat on the fabrication piston is essential for several reasons. Firstly, uneven heat can lead to uneven heating of the powder material, which can cause warping or deformation of the printed parts. This can result in poor dimensional accuracy. Secondly, uneven heat can also cause uneven sintering of the powder material. If some areas of the fabrication piston are not heated enough, the powder may not sinter properly, resulting in weak or porous parts. Lastly, uneven heat can also cause uneven stress and strain distribution during the cooling process, leading to cracking and deformation of the final product. A Fluke thermal imaging camera was used to test the heat distribution over the fabrication piston in this SLS printer. The heat chamber temperature was set to 160°C; the results are shown in Figure 25 below.

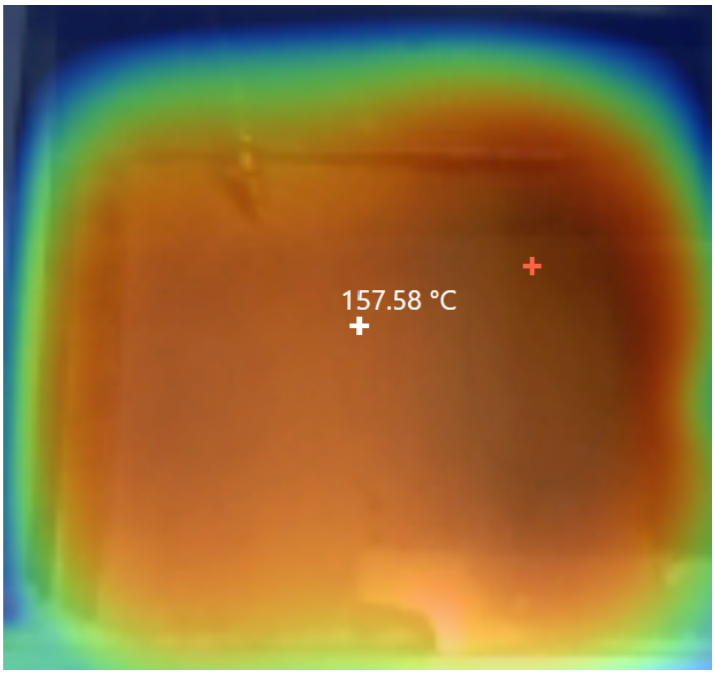


Figure 25: Heat Bed Validation

After heating up for around 25 minutes, the Fluke IR camera indicated that the fabrication has a distribution temperature of 157.58°C. This measurement was close to the set temperature of 160°C, and differences could have been attributed to calibration errors.

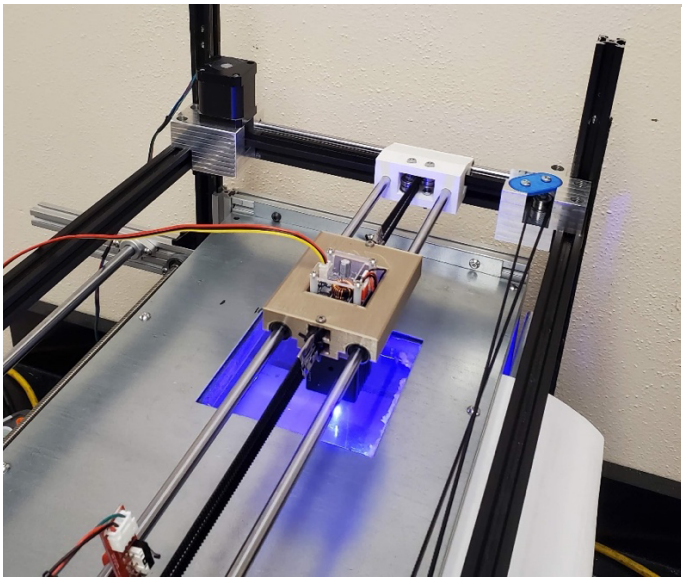




Figure 26: Aluminum Alloy 4W Laser Engraver

The laser attached to the gantry system is an aluminum alloy 4W laser engraver. It has an adjustable focus between 20-35mm, with a 450 nm laser head. This laser is connected to the Duet board via Pulse Width Modulation (PWM). In PWM control, the signal consists of a series of pulses with a fixed period, and the width of each pulse is varied to control the average voltage or current delivered to the laser. The effective voltage or current supplied to the device can be adjusted by varying the pulse width. The Duet 3D Mini 5+ Wi-Fi board supports a pulse width range of 0 to 1, with a resolution of 12 bits (4096 steps), allowing for very fine control over the output voltage or current.

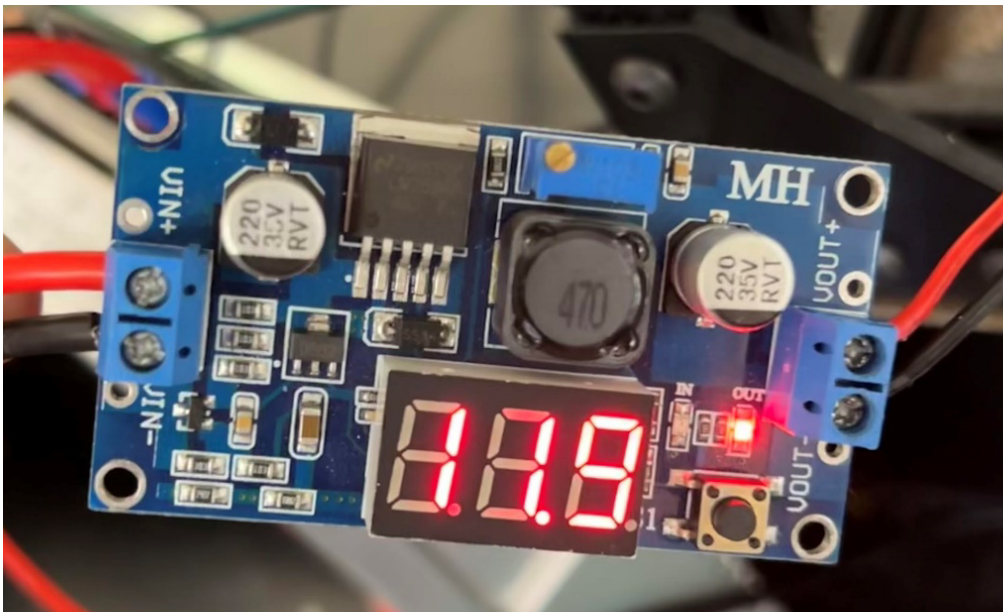


Figure 27: 24V to 12V Buck converter

A buck converter connects the power source to the laser, decreasing the voltage from 24V to 12V. A buck converter is a DC-to-DC converter that reduces the input voltage to a lower output voltage. It works by switching a power transistor on and off at a high frequency, allowing a small amount of energy to be transferred to the output during each switching cycle. This was added so the laser could draw power from the power source, not the Duet board.

Section 2.4 Software Configuration

The configuration for this board begins with the Duet online configuration tool, which generates configuration files based on the user-input number of axes, heaters, fans, expansion boards, etc. This tool does not, however, allow for more specific configurations that this SLS printer requires. As such, the generated configuration file was manually edited to include another Z-axis for the second piston, a linear axis for the sweeper arm movement, and other SLS customizations. These edits were done by referencing the original configuration file and using the Marlin G-Code command library shown in Table 2 below.

Table 2: Marlin G-Code Command Library

Movement Type	Marlin Command
X	G1 X#*
Y	G1 Y#*
Sweeper arm	G1 U#*
Fabrication piston	T0 or G1 Z#*
Delivery piston	T1 or G1 Z#*
Laser activation	M106 S#**
Laser deactivation	M107

Anywhere a # is shown, a location where a variable integer can be inserted.

* The variable here denotes the distance the axis moves

**The variable integer insertion here determines the power allotted to the laser and can be increased if it needs more power. When the laser intensity is set to 0, the laser is off, and no sintering occurs. As the intensity increases, more energy is delivered to the powder particles, with the max intensity being 255.

The following general preferences and network settings for the board were left from the original configuration file shown in Figure 28 below. These settings send absolute axis

coordinates to preserve the location of the gantry system, set a custom printer name as “SLS Printer,” and select a Core XY gantry system movement. The network settings are also set to allow HTTP network connection for wireless control. These settings are a foundation for the entire printer, allowing customized movements and commands.

```
; General preferences
G90                                 ; send absolute coordinates...
M83                                 ; ...but relative extruder moves
M550 P"SLS Printer"                 ; set printer name
M669 K1                             ; select CoreXY mode

; Network
M552 S1                             ; enable network
M586 P0 S1                          ; enable HTTP
M586 P1 S0                          ; disable FTP
M586 P2 S0                          ; disable Telnet

; Drives
M569 P0.0 S1                        ; physical drive 0.0 goes forwards (X)
M569 P0.1 S1                        ; physical drive 0.1 goes forwards (Y)
M569 P0.2 S0                        ; physical drive 0.2 goes forwards (Z1 - build)
M569 P0.3 S1                        ; physical drive 0.3 goes backwards (Z2 - powder)
M569 P0.4 S0                        ; physical drive 0.4 goes forwards (arm)
M584 X0.1 Y0.0 Z0.2:0.3 U0.4        ; set drive mapping. x,y, two z, and U for arm
M350 X16 Y16 Z16 U16 I1             ; configure microstepping with interpolation
M92 X80.00 Y80.00 Z4000.00 U1500.00 ; set steps per mm
M566 X900.00 Y900.00 Z45.00 U100.00    ; set maximum instantaneous speed changes (
M203 X6000.00 Y6000.00 Z300.00 U1000.00 ; set maximum speeds (mm/min)
M201 X500.00 Y500.00 Z25.00 U100.00    ; set accelerations (mm/s^2)
M906 X800 Y800 Z800 U800 I30        ; set motor currents (mA) and motor idle factor i
M84 S30                             ; Set idle timeout
; Axis Limits
M208 X-140 Y0 Z-10 U-10 S1          ; set axis minima (need change by offset)
M208 X140 Y100 Z80 U380 S0        ; set axis maxima (need change by offset)

; Endstops
M574 X1 S1 P"!io0.in"              ; configure switch-type (e.g. microswitch) endstop for low end on X
M574 Y1 S1 P"!io1.in"              ; configure switch-type (e.g. microswitch) endstop for low end on Y
M574 Z1 S1 P"!io2.in"              ; configure switch-type (e.g. microswitch) endstop for high end on Z
M574 U1 S1 P"!io3.in"              ; configure switch-type (e.g. microswitch) endstop for low end on U
```

Figure 28: Custom Duet Configuration File Code

Two drivers were added to the configuration under the "Drives" area in Figure 28. These settings activate a positive motion axis for the sweeper arm and a negative one for the second piston. The second piston, the powder/delivery piston or Z2 axis, has its direction value set backward using the S0 command instead of the S1 command. Though, later commands put it to the same driver as the other piston axis, which makes both piston axes move by the same

commands and amount but in opposite directions. This ensures that the volume added per layer equals that of powder swept onto the fabrication plate.

After the additional driver settings, the M584 command sets the drive mapping shown in Figure 28. This assigns the axes to the pin locations, using pins 0.3 for the delivery piston Z2 axis and 0.4 for the sweeper arm U axis, in addition to the already generated pin locations for the X, Y, and Z1 motors. The motor settings are then defined: steps per millimeter, maximum speed change, maximum speed, acceleration, and current for each motor. After these changes, each axes' size is defined by its minima and maxima using the M208 command under the "Axis Limits" area. Then, two end stops are added to the original configuration file, one each for the Z2 and U axis, and all are defined as switch-type end stops shown in the area labeled "Endstops."

```
; Z-Probe
M558 P0 H5 F120 T6000            ; disable Z probe but set dive height, probe speed and travel sp
M557 X15:215 Y15:195 S20         ; define mesh grid

; Heaters
M140 H-1                         ; disable heated bed (overrides default heater mapping)

; Fans

; Tools
M563 P0 S"Laser"    ; define tool 0
G10 P0 X0 Y0 Z0     ; set tool 0 axis offsets
G10 P0 R0 S0     ; set initial tool 0 active and standby temp 0c

; Custom settings
M452 C"out6" R255 F200           ; Eable Laser mode, on out6, with max intensity being 255, with
```

Figure 29: Duet Configuration File Laser Code

Figure 29 shows the configuration code that disables the Z-probe code, as this printer does not use one, and disables all heaters, fans, and tools. The configuration is modified for an SLS printer by defining the printer as being in laser mode using the M452 command. This command defines the pins of the laser PWM output and its characteristics of having an intensity range of 0-255 and a PWM frequency of 200 Hz.

When generating linear movement of the gantry system in the X direction, the configuration file will automatically activate both motors in the opposite direction, causing both belts to move in the opposite direction since the printer uses a CoreXY gantry system. Both motors are activated in the same direction for movement in the Y direction, which moves the belts in the same direction, as discussed in Section 2.2. This movement is summarized in Table 3 below.

Table 3: Core-XY Coordinate Movement Based on Motor Rotation

Coordinate Movement	**Direction of Left Motor**	**Direction of Right Motor**
+X	Ccw	Cw
-X	Cw	Ccw
+Y	Ccw	Ccw
-Y	Cw	Cw

After the essential functions of the printer are registered within the Duet board, the printer will be able to take commands to control all the processes. These processes allow the printer to start printing, which consists of 4 steps outlined in Figure 30.

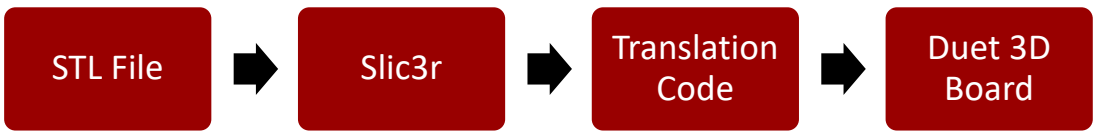


Figure 30: Diagram of the Steps in the Printing Process

The first step in printing is to create a 3D part and export it as an STL file. An STL (STereoLithography) file is a format commonly used for 3D printing. It is a simple format representing a 3D object as a set of triangular faces. STL files can be created using various 3D modeling software, such as SolidWorks, AutoCAD, Blender, etc. For this thesis, all sample models were made in SolidWorks 2022 and exported as an STL file.

Once an STL file has been created, the second step is to import the file into a slicing software called Slic3r. Slic3r takes the STL file, breaks it down into 2D layers of a defined thickness, and creates a path for the laser to follow its contours and infill areas. The slicer configuration file was edited to define the startup and end of print and layer changes. The startup process in the configuration file was edited to optimize the slicing process for SLS printing rather than extrusion. This configuration removes extruder heating since this printer uses a laser. Homing has also been added for the sweeper arm and the powder delivery piston. Homing for the powder piston is prevented from resetting, as the level set at the beginning of the print process is assumed to be zero. This facilitates filling the powder piston with sugar, as different amounts can be used. It is also assumed that the printer is started having a leveled powder piston. In addition, a code block is inserted at each layer change to facilitate the SLS process. For each layer change, the slicer inputs G-Code to raise the powder delivery piston, lower the fabrication piston, move the sweeper arm to the fabrication piston to add a new layer of powder, then return the sweeper arm to home. The pseudocode for this change is shown in Figure 31 below.

```
G1 Z#     ; Move powder piston up, and fabrication piston down
G1 U370   ; Move sweeper arm across fabrication to the right
G1 U0     ; Move sweeper arm back to home on the left
```

Figure 31: Layer Change Pseudocode

After Slic3r generates the G-Code with the SLS configurations, it is put through an SLS G-Code coordinate translation program for the third step. This translation program was written in C++ and searches the G-Code line by line, replacing all the extrusion commands denoted with 'E' to laser activation 'S.' As shown in Table 2, the 'S' command activates the laser, followed by an integer determining the intensity sent to the laser. In addition to replacing the extrusion commands, this translation program can conveniently adjust the laser intensity. This helps adjust printing parameters and printing materials that require different laser intensities to sinter.

```
// prepare files to read and write
string infilename = "Leaf_GCode_S175_F45.gcode";
string outfilename = "translated_" + infilename;
fstream infile; fstream outfile;
infile.open("\\Users\\jacob\\OneDrive\\Desktop\\SLS\\Gcode Generation\\Leaf_GCode_S175_F45.gcode", ios::in);
outfile.open(outfilename, ios::out);

string on = "S175"; //GCode command for activating laser
```

Figure 32: Adjusting Laser Intensity

```
size_t posE = line.find('E'); //find location of E command
if (posE < 30 && (isdigit(line[posE + 1]))) // if found on line with extrusion
{
    e = stof(line.substr(posE + 1, posE + 6)); //find e value
    //cout << e << "\n";
    if (e > 0) // positive extrusion
    {
        outfile << line.substr(0, posE) << on << "\n";// movement command without E, adding S
    }
    else
    {
        outfile << line.substr(0, posE) << "\n"; // movement command without E command
    }
}
else if (posE < 30 && (line[posE + 1] == '-')) // found on line with negative extrusion
{
    outfile << "\n";
    //outfile << line.substr(0, posE) << "\n"; // movement command without E command
}
else // if no extrusion command
{
    outfile << line << "\n"; // print original line
}
```

Figure 33: Laser Activation Command Replacement Code

The blocks of code shown in Figure 32 and Figure 33 above are run in Microsoft Visual Studio. The first part of the translation code shown in Figure 32 opens the sliced G-Code file

from the location it was exported to from Slic3r. The last line in Figure 32 initiates a string variable called “on” and stores the ‘S’ command followed by the numeric laser intensity value with which the program will replace the ‘E’ commands.

The algorithm shown in Figure 33 searches and replaces extrusion, ‘E’ commands, with laser ‘S’ commands. If a positive integer follows the ‘E’ command, indicating material addition, it removes it and inserts the “on” variable that stores the laser ‘S’ command and its intensity. A zero or negative value following the ‘E’ command represents no extrusion, so no laser activation is inserted. If no ‘E’ command or an integer does not follow an ‘E’ command, the original code line is added to the translated G-Code file without alteration. The final printing step is to upload the translated G-Code file onto the Duet interface through Wi-Fi.

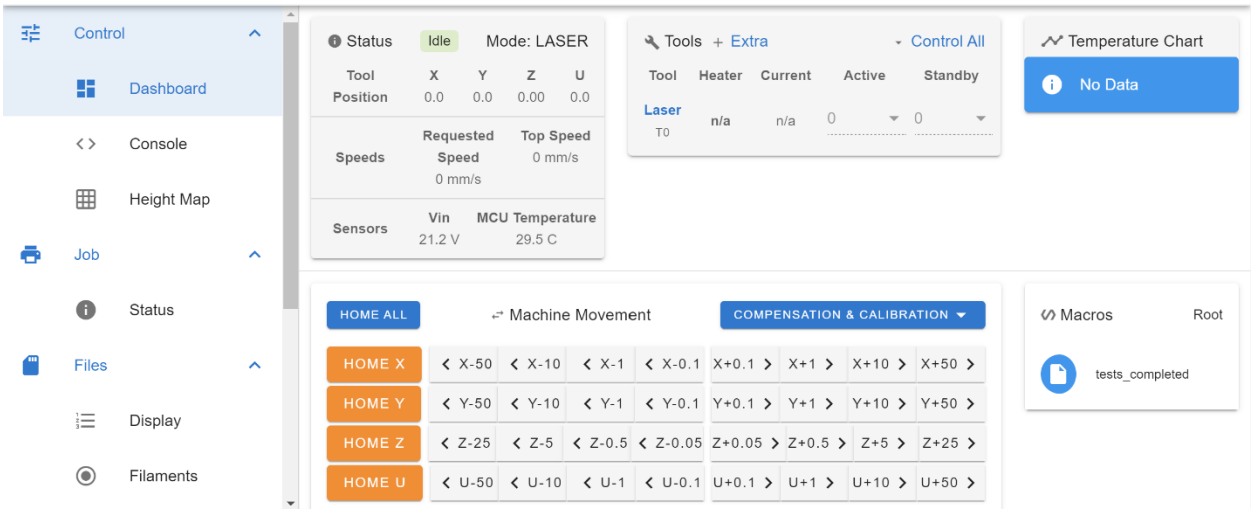


Figure 34: Controlling Printer Movement in Duet Interface

The 4 axes of the printer can be manually adjusted and homed through the Duet 3D interface dashboard. Other essential metrics are shown, such as the laser position and speed. After the printer’s axis is homed, the translated G-Code file can be uploaded and started within the interface.

Section 2.5 Printer Optimization

Print optimization for an SLS 3D printer involves several techniques and strategies to improve the quality and efficiency of the printing process. Critical optimization techniques include proper bed leveling, correct material selection, and fine-tuning the laser intensity and scanning speed. To ensure an even heat distribution and consistent powder sintering, it is essential to level the fabrication piston accurately. This can be done by adjusting the piston height and ensuring the bed is free from debris or powder buildup. Choosing the appropriate powder material for the application can also significantly impact the printing process's quality and efficiency. Some powders are better suited for specific applications and can result in higher resolution and more robust parts. This printer is designed to print sugar, and it is critical to buy pure cane sugar that does not contain other ingredients like some baking sugars.



Figure 35: Pure Cane Sugar

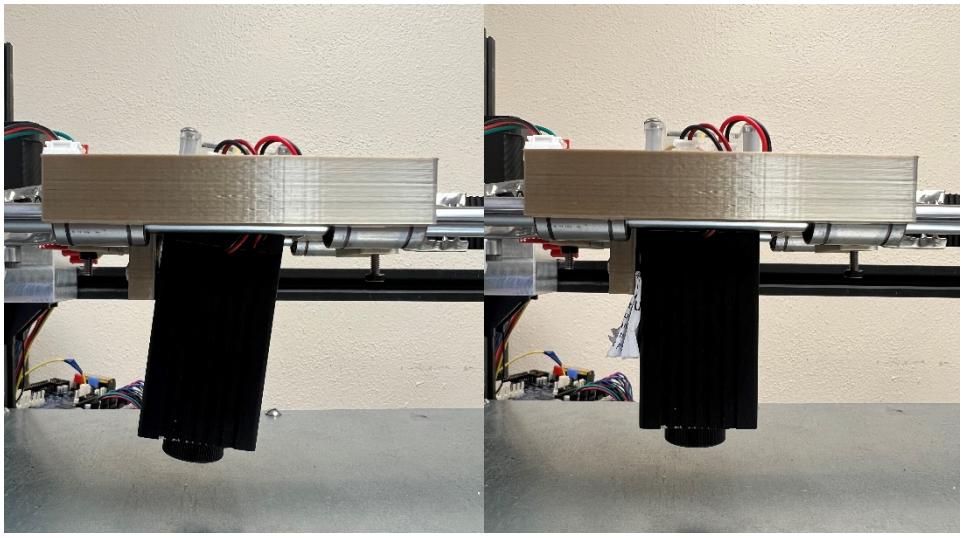


Figure 36: Slanted Laser Position

Several issues can arise if a laser is incorrectly positioned when sintering material. If the laser does not hit the target area accurately, the sintering process may not be completed. This can result in weak or incomplete sintering and poor material quality and performance. The second issue is over-sintering. If the laser is positioned incorrectly and remains in one spot for too long, it can overheat the material, resulting in over-sintering. This can cause the material to become brittle or even crack, compromising its strength and durability. The third issue is that it can cause the material to deform or warp, resulting in misshapen parts that do not meet the required specifications. The laser position was adjusted to a 90-degree angle to mitigate these potential issues using a piece of folded paper, as shown in Figure 36. This change was essential to achieve optimal results and prevent any issues arising from incorrect positioning. Another technique was to let the sugar heat up an extra 15 minutes before printing. This ensured that all the sugar reached the desired temperature set by the heat chamber before being sintered.

Chapter 3: 3D Printing of Sugar Samples

Section 3.1: Sample Modeling and G-Code Generation

Each sample was designed and exported as an STL from SolidWorks 2022. They were then sliced in an open-source slicing software called Slic3r. Slic3r then generates the G-Code based on the slicing settings and the 2D layers. Then, the G-Code was run through the translation program to adjust the code for this SLS printer. Each of the figures below includes the SolidWorks model and the laser toolpath. Section 2.4, Software Configuration, outlines the G-Code generation process in more detail.

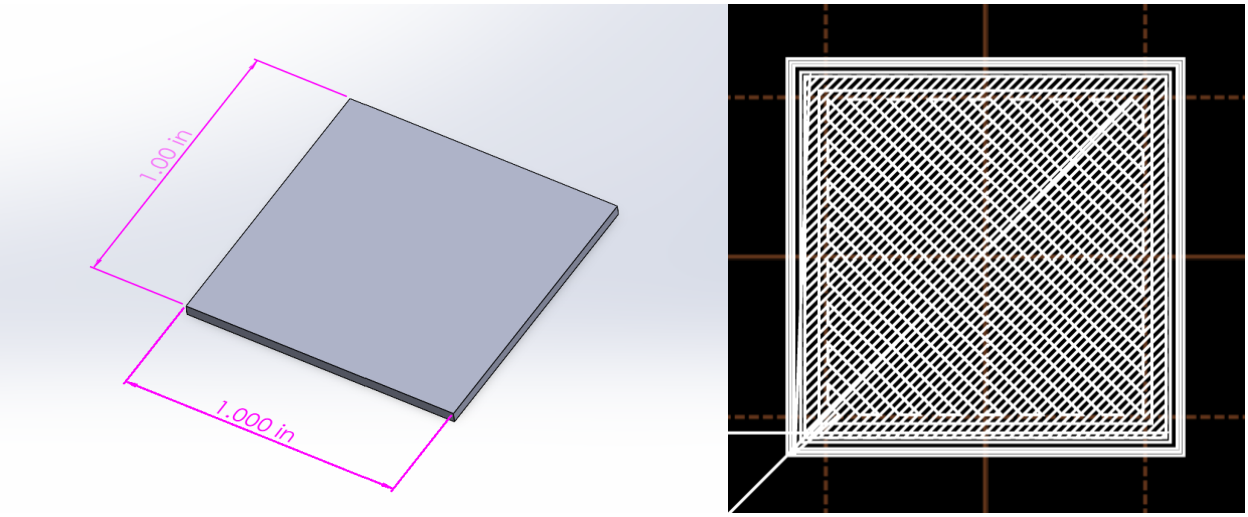


Figure 37: Square Sample Generation

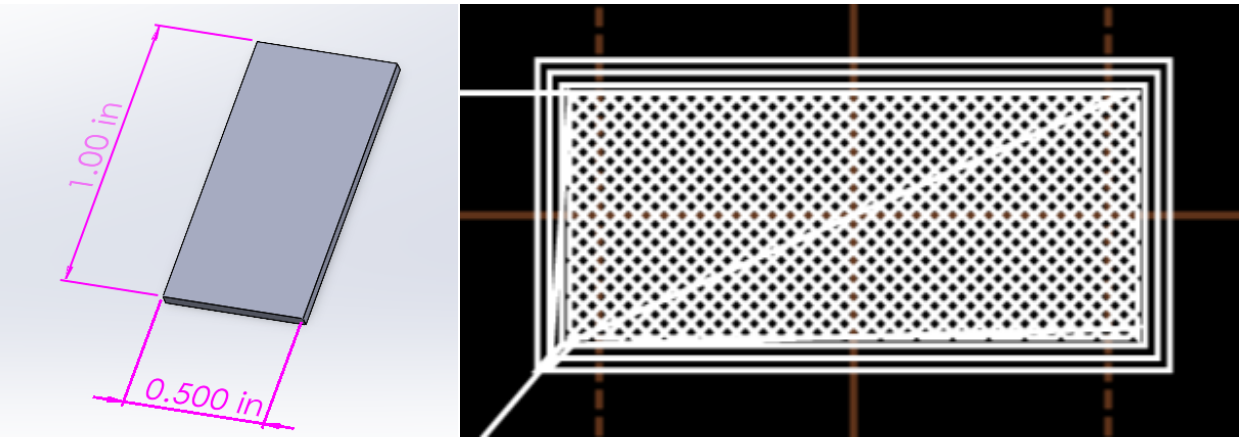


Figure 38: Density Test Sample Generation

The first two samples are shown in Figure 37 and Figure 38 and were designed to show that this printer can print a simple 2D geometry. A square will test how the laser performs when sintering the sharp corners and how well it can sinter the inside of the square. This sample helped modify the printing parameters to optimize them. The second sample, the density test sample, was designed to be placed into a pycnometer. This sample has a smaller geometry that would fit better into the sample chamber within the pycnometer. After generating the first two samples, more complex geometries were designed to showcase the printer's potential.

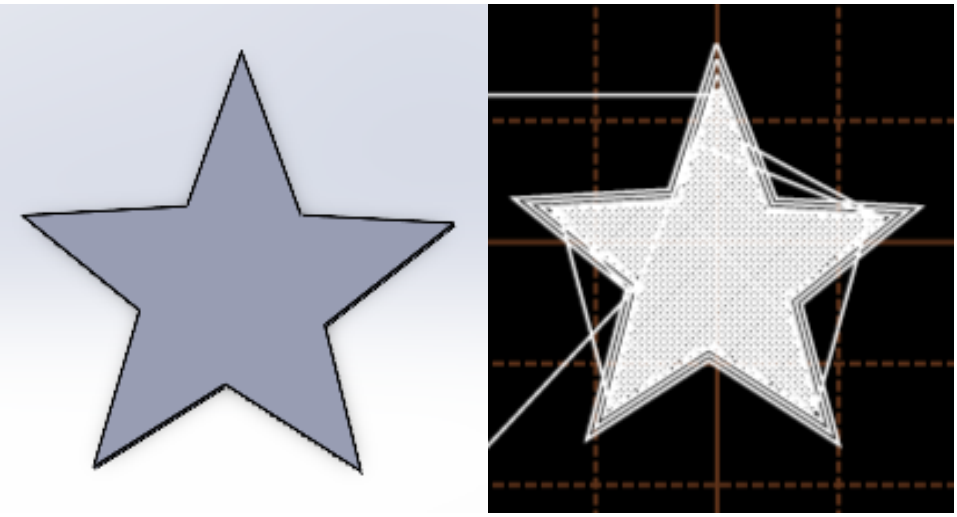


Figure 39: Star Sample Generation

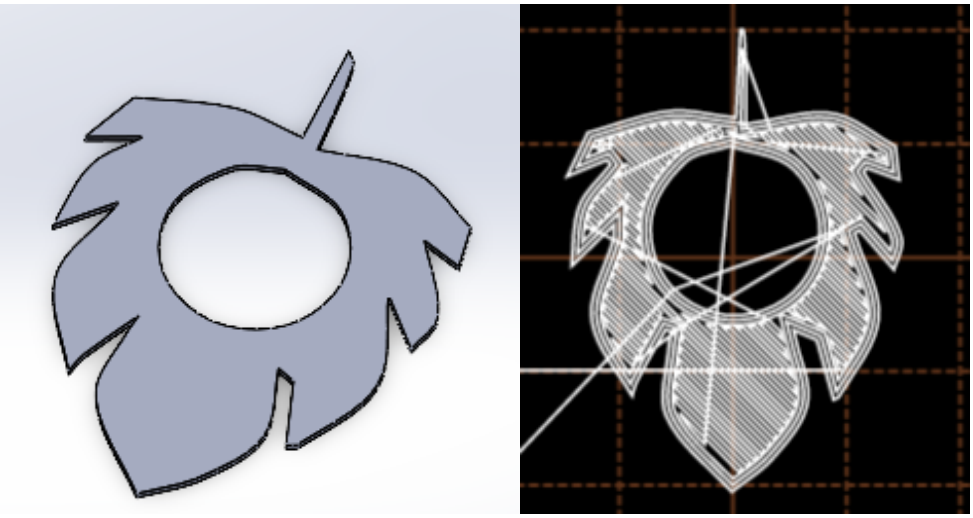


Figure 40: Leaf Sample Generation

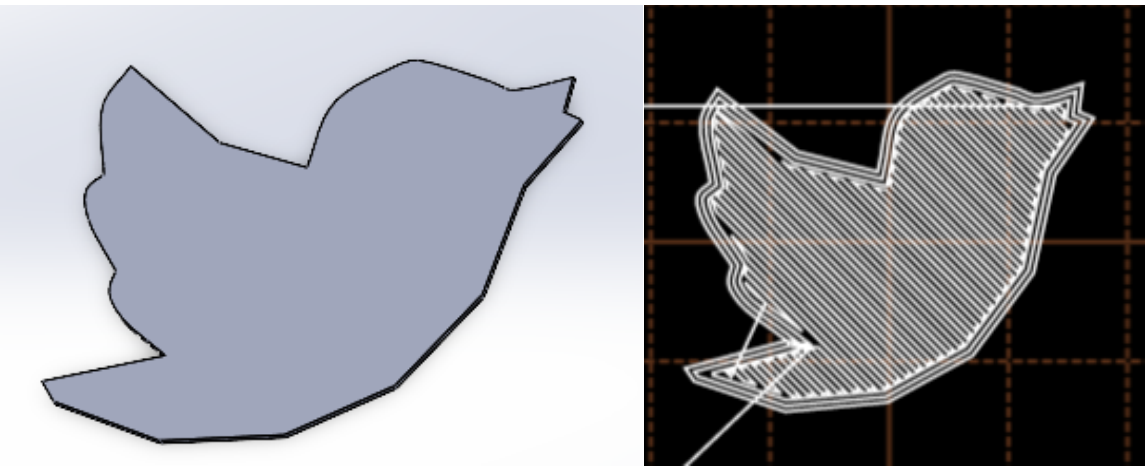


Figure 41: Bird Sample Generation

The last three samples are shown in Figure 39, Figure 40, and Figure 41. The first sample is a picture of a star, which is relatively simple but has more complex geometry than the square. One of the most important things this sample showcases is the strength of the sintered sugar bonds, especially at the star's tips. The following leaf sample shows that the printer can sinter tiny areas without bonding the other sugar, such as the crevasses on the leaves. It also shows that it can sinter around the center hole without bonding the sugar in the hole. The last sample is the bird sample. This sample has the most complex geometry and showcases the printer's potential. Being able to print detailed geometries like the bird sample shows that this printer can continue to be upgraded for more advanced biomedical engineering applications in the future.

Section 3.2: Printing Parameters

The laser power, scanning speed, and heat chamber temperature are critical parameters affecting the printing process's quality and efficiency. The laser scanning speed is the speed at which the laser scans across the surface of the sugar, and the laser intensity is the voltage that the laser receives from the PWM port. The appropriate laser scanning speed and power depend on several factors, including the material type, the part's size and complexity, and the desired resolution. Typically, a slower scanning speed and higher intensity will result in a more precise and detailed part but will also take longer to print. These parameters are adjusted to ensure the sugar is sintered correctly so that the parts are not burned or under-sintered.

There are a total of 12 samples printed for this thesis. This includes three square samples, three density test samples, two star samples, two leaf samples, and two bird samples. Each printing parameter was adjusted based on the result of the previous samples. Minor adjustments were made if the sample was not appropriately sintered enough. For example, in Table 4, the scanning speed and heat chamber were decreased, while the laser intensity was increased after each sample. The tables below outline the printing parameters for each of the 12 samples. The pictures of the samples are in the next section, starting in Figure 42.

Table 4: Printing Parameters for Square Samples

Sample	Scanning Speed	Laser Intensity (Max 255)	PWM Voltage (Max 5V)	Time to Complete Print	Heat Chamber Temperature
Square 1	1mm/s	240	4.7V	0:55:52	160°C
Square 2	0.75mm/s	245	4.8V	1:14:29	155°C
Square 3	0.5mm/s	250	4.9V	1:51:41	150°C

Table 5: Printing Parameters for Density Test Samples

Sample	Scanning Speed	Laser Intensity (Max 255)	PWM Voltage (Max 5V)	Time to Complete Print	Heat Chamber Temperature
Density Test 1	0.5mm/s	250	4.9V	0:56:20	155℃
Density Test 2	0.5mm/s	250	4.9V	0:56:20	150℃
Density Test 3	0.5mm/s	250	4.9V	0:56:20	145℃

Table 6: Printing Parameters for Star Samples

Sample	Scanning Speed	Laser Intensity (Max 255)	PWM Voltage (Max 5V)	Time to Complete Print	Heat Chamber Temperature
Star 1	0.5mm/s	250	4.9V	1:14:54	150℃
Star 2	0.5mm/s	250	4.9V	1:14:54	145℃

Table 7: Printing Parameters for Leaf Samples

Sample	Scanning Speed	Laser Intensity (Max 255)	PWM Voltage (Max 5V)	Time to Complete Print	Heat Chamber Temperature
Leaf 1	0.5mm/s	245	4.8V	1:35:30	150℃
Leaf 2	0.5mm/s	245	4.8V	1:35:30	145℃

Table 8: Printing Parameters for Bird Samples

Sample	Scanning Speed	Laser Intensity (Max 255)	PWM Voltage (Max 5V)	Time to Complete Print	Heat Chamber Temperature
Bird 1	0.5mm/s	250	4.9V	1:38:00	145℃
Bird 2	0.5mm/s	250	4.9V	1:38:00	140℃

Section 3.3 Simple Single-Layer Samples

The purpose of the simple single-layer samples is to determine the best printing parameters. Determining the sugar's ideal heat chamber temperature, laser scanning speed, and laser intensity is necessary before attempting more complex geometries. The first three printed samples were 1x1in square samples. This is the most basic single-layer geometry, making fine-tuning printing parameters easier. Table 4 above shows the printing parameters for the square samples shown in Figure 42 below.

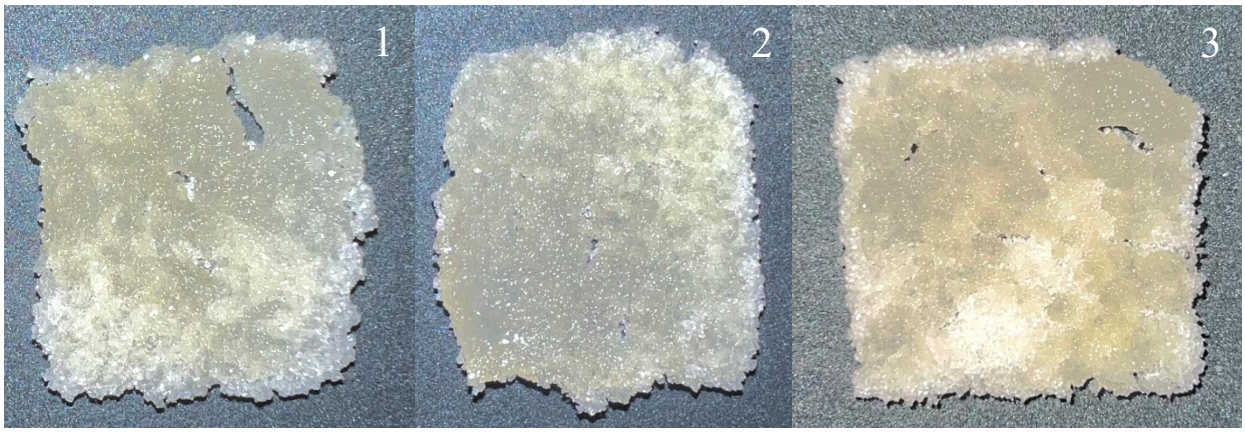


Figure 42: Square Samples

Since the heat chamber temperature was 160℃, meaning the sugar was about 20℃ below the sintering temperature, a slow scanning speed of 1mm/s and a high laser intensity of 240 were selected for the first sample. The first sample performed better than expected, as it could be removed from the fabrication piston and hold its shape. However, it has some visible imperfections, especially the sugar not properly sintered in the top right. This sample was a promising start and demonstrated that this technology could properly sinter sugar. The second sample improved after decreasing the scanning speed to 0.75mm/s, decreasing the heat chamber temperature to 155℃, and increasing the laser intensity to 245. This sample had a much better infill but did not have accurate corners. To mitigate this, the scanning speed was reduced even

further to 0.5mm/s, the heat chamber temperature was decreased to 150℃, and the laser intensity was increased to 250 for the third sample. These adjustments sintered the sharp corners more accurately. Unfortunately, while removing the third sample from the fabrication piston, the top right-hand corner was accidentally brushed off, causing a tiny hole in the top right to form. Regardless, the printing parameters used in the third sample were determined to be the best and served as a baseline for the remaining samples.

The following three printed samples are printed to fit into a pycnometer for a density test discussed in Section 4.2: Density Test. This sample is 0.5x1in, effectively half of the 1x1in square samples.

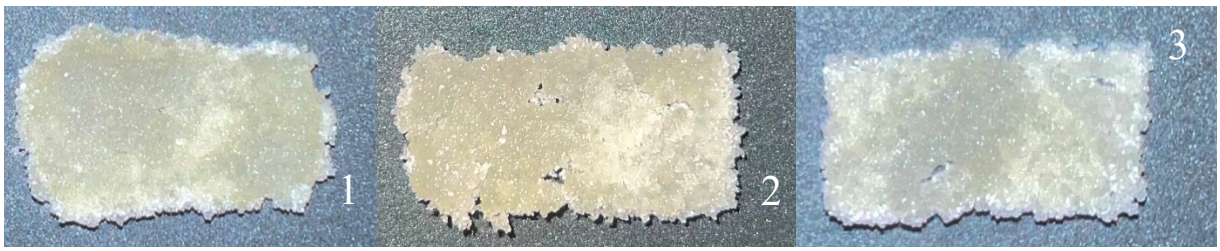


Figure 43: Density Test Samples

The starting scanning speed for the first density test sample was 0.5mm/s, with a 250 laser intensity and a heat chamber temperature of 155℃, which were derived from the parameters from the third square sample. The first sample appeared to be over-sintered and melted toward the top. This was solved in the second sample as the heat chamber temperature was decreased to 150℃. Sample 2 had much better corners but still was not sharp enough and is inaccurately sintered in some areas. For the third sample, the heat chamber temperature was reduced another 5℃ to 145℃. This was the overall best density test sample. It had a smooth infill and properly sintered corners. These six samples helped determine the best printing parameters for complex geometry single-layer samples shown in the next section.

Section 3.4: Complex Single-Layer Samples

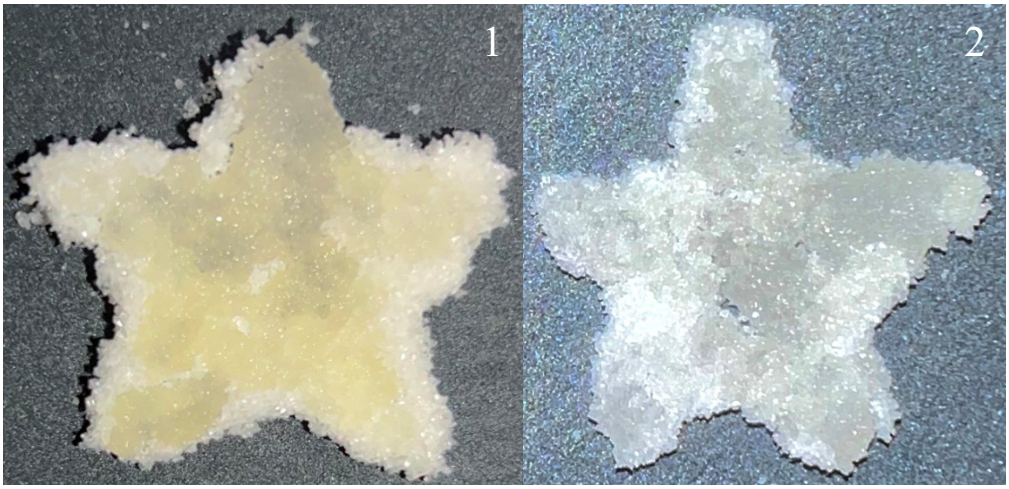


Figure 44: Star Sample

The starting scanning speed for the first star sample was 0.5mm/s, with a 250 laser intensity and a heat chamber temperature of 150℃. A lot of extra sugar was not brushed off, which can be seen by the light-colored sugar on the perimeter. This caused the sample to look less accurate than it was. The sample was also dark yellow, which indicates that the sugar was slightly over-sintered. For the second sample, the heat chamber temperature was decreased to 145℃ to help reduce the amount of sintering. This sample looked better, but some ends of the star were brushed off when removing the sugar from the perimeter.



Figure 45: Leaf Sample

The starting scanning speed for the first leaf sample was 0.5mm/s, with a 250 laser intensity and a heat chamber temperature of 150℃. The first sample appeared over-sintered and brittle, seen by the dark yellow color and cracks. To mitigate this for the second sample, the heat chamber temperature was decreased to 145℃. It appeared a lot smoother and was an overall better print. One of the most impressive features of this print was sintering the sugar around the center ring without sintering the sugar on the inside and sintering the small areas around the leaf. This showcased that this printer was able to print complex geometries.

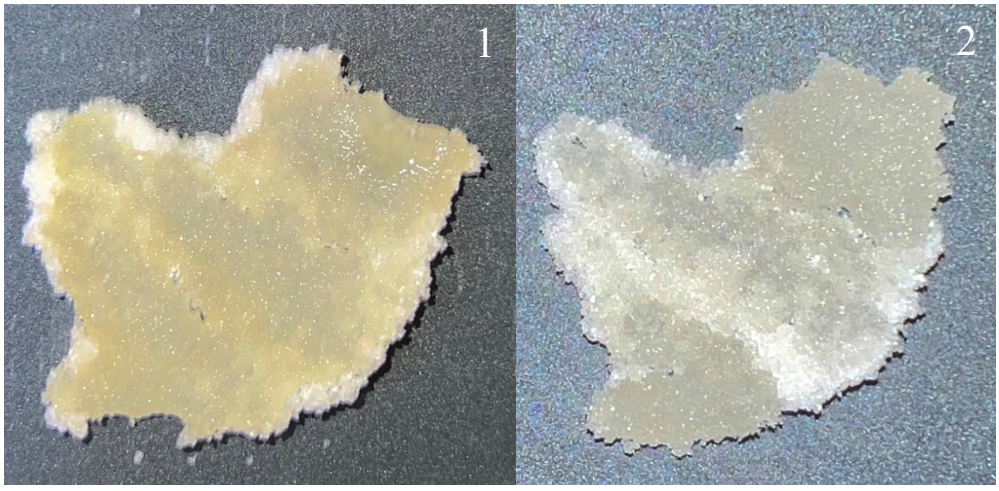


Figure 46: Bird Sample

The starting scanning speed for the first bird sample was 0.5mm/s, with a 250 laser intensity and a heat chamber temperature of 150℃. The first sample was way over-sintered, as seen by its dark yellow color. To address this for the second sample, the heat chamber temperature was decreased to 145℃, like the second star and leaf sample. This sample was by far the most impressive from this printer. This sample has detail and structure. This sample inspires future research to continue printing complex geometries in two and eventually three dimensions.

Chapter 4: Measurement and Geometry Shape Validation

Section 4.1: Sample Measurements

This section evaluates the mass of all twelve samples and the area of the six simple single-layer samples. Figure 47 below incorporates the masses of the simple single-layer samples outlined in Table 9.

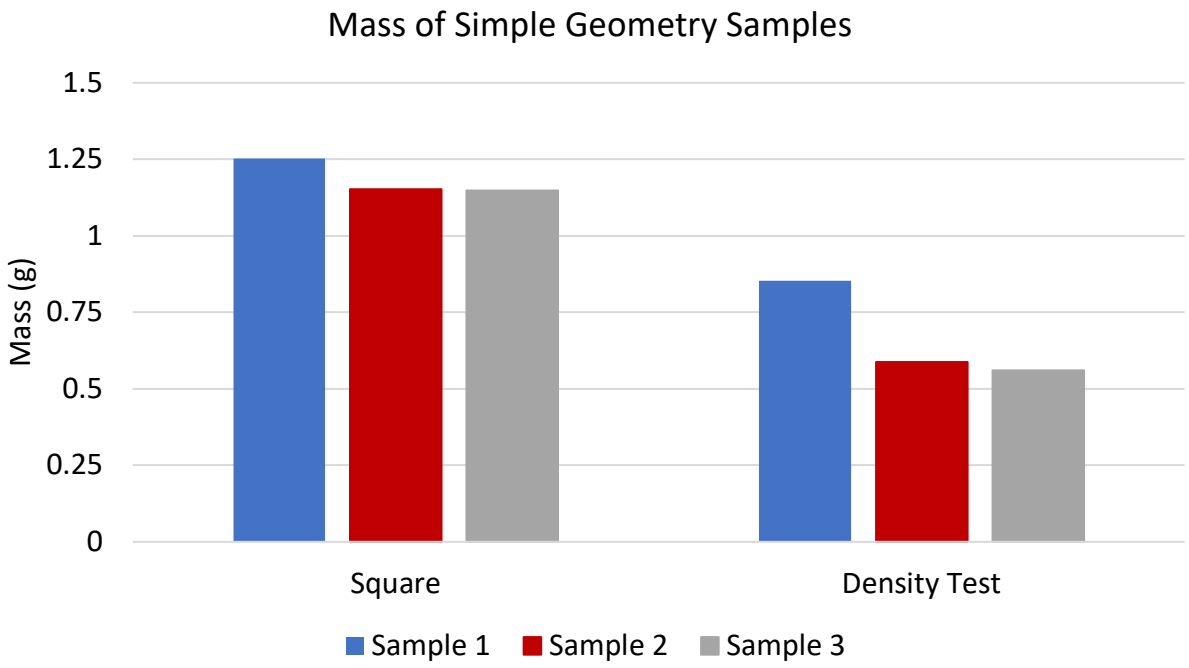


Figure 47: Chart of Simple Single-Layer Samples

Table 9: Mass of Single Layer Samples

Sample	Sample 1	Sample 2	Sample 3
Square	1.252g	1.152g	1.148g
Density Test	0.853g	0.588g	0.560g

The first samples for the square and density test samples weigh the most compared to the other samples. They were the most over-sintered samples, as discussed in the previous section. The heat chamber temperature was too high for those samples, which caused them to sinter more

of the surrounding sugar than necessary. The other two square and density test samples had similar masses. They looked more alike, showing that decreasing the heating chamber temperature and scanning speed while increasing the laser intensity caused more precision sintering.

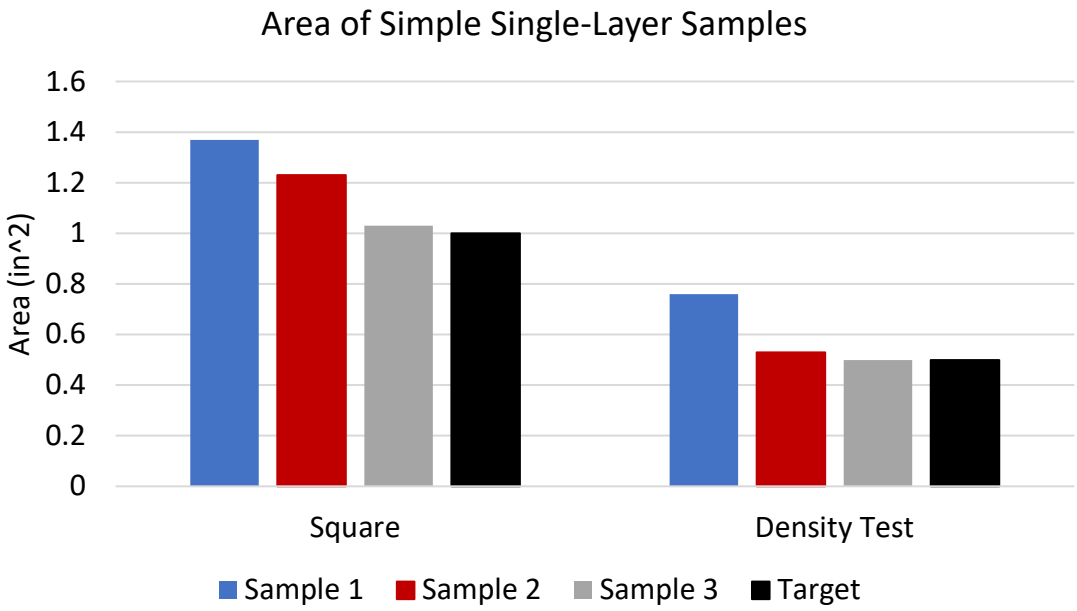


Figure 48: Area of Simple Single-Layer Samples

Table 10: Area of Simple Single-Layer Samples

Sample	Sample 1	Sample 2	Sample 3	Target
Square	$1.37in^2$	$1.23in^2$	$1.03in^2$	$1in^2$
Density Test	$0.76in^2$	$0.53in^2$	$0.5in^2$	$0.5in^2$

Figure 48 and Table 11 above show the area of the six simple single-layer samples. The values were calculated by measuring the samples' length and width using a pair of calipers and multiplying them. The square sample is 1x1in, so the target area is $1in^2$. The density test sample is 0.5x1in, so the target area is $0.5in^2$. Like the conclusions drawn from the mass measurements above, the first samples for the square and density tests were over-sintered, which explains why

the area is so far off the target. The third square sample was the closest to the target area of the square, with an area of $1.03in^2$. Likewise, the third density test sample was the closest to the target, with an area of $0.5in^2$.

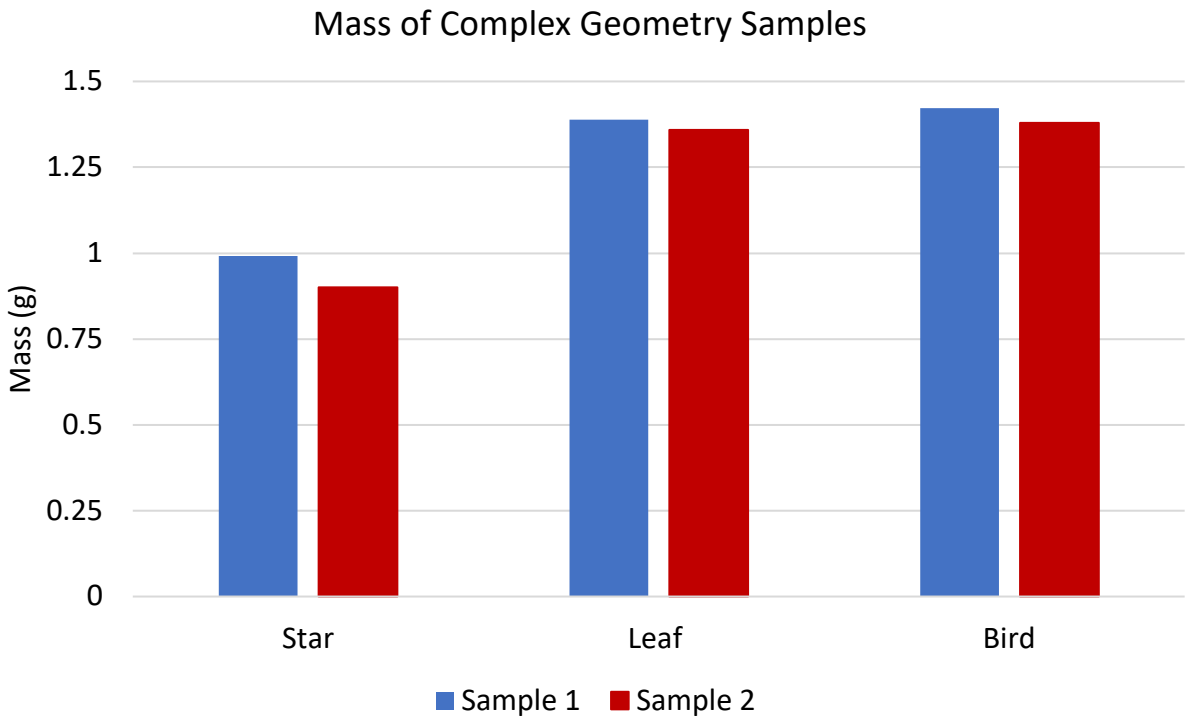


Figure 49: Chart of Complex Geometry Single-Layer Samples

Table 11: Mass of Complex Geometry Samples

Sample	Sample 1	Sample 2
Star	0.992g	.901g
Leaf	1.389g	1.358g
Bird	1.423g	1.380g

Figure 49 above incorporates the masses of the complex single-layer geometries outlined in Table 11. The first sample for all three geometries weighed more than the other sample like

the simple single-layer geometries. This was attributed to over-sintering, as discussed in the previous section. The mass and measurement results indicate that the most accurate samples were printed with a scanning speed of 0.5mm/s, a 250 laser intensity, and a heat chamber temperature of 145-150℃. This printer can print simple and complex geometry single-layer samples with impressive accuracy, which will be utilized for future research in biomedical engineering applications.

Section 4.2: Density Test



Figure 50: AccuPyc II 1340 Gas Pycnometer to Measure the Density Test Samples

The AccuPyc II 1340 gas pycnometer is a device used to measure the density of solids, powders, and other materials. It measures the volume of gas displaced by a material sample in a sealed chamber. The smallest sample that could be placed into the pycnometer was the density test sample shown in Figure 43. After the sample chamber was cleaned with acetone and dried, the sample chamber was installed into the pycnometer. Then, the pycnometer was calibrated, which is essential for accurate measurements. The sample was then placed into the chamber, closed, and tightly sealed. When the test starts, the pycnometer measures the volume of gas displaced by the sample and calculates the density of the sample based on the sample's mass shown in Table 5.

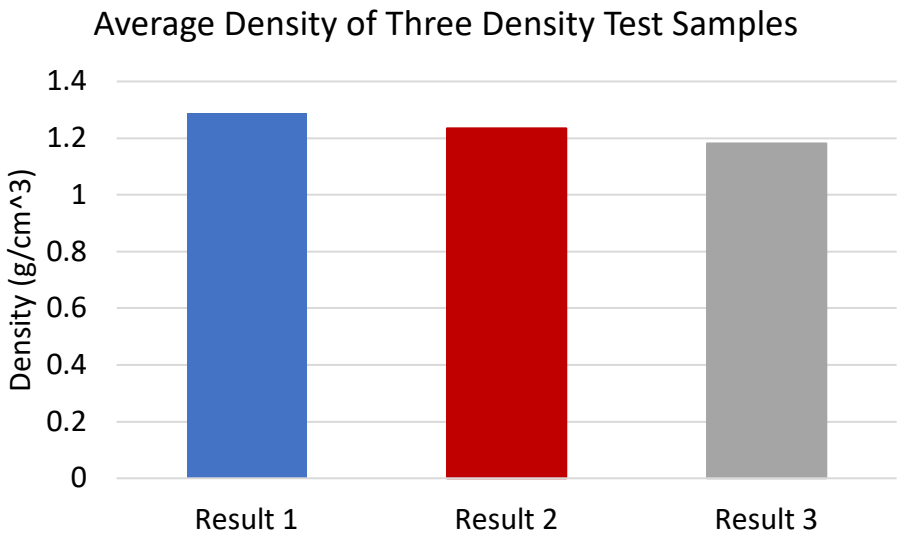


Figure 51: Average Density of Three Density Test Samples

Table 12: Density Test Sample Volume

Measurement	Result 1	Result 2	Result 3
Average	0.6626 cm^3	0.4763 cm^3	0.4744 cm^3
Standard Deviation	0.0028 cm^3	0.0028 cm^3	0.0118 cm^3

Table 13: Density Test Sample Density

Measurement	Result 1	Result 2	Result 3
Average	1.2873 g/cm^3	1.2345 g/cm^3	1.1812 g/cm^3
Standard Deviation	0.0054 g/cm^3	0.0073 g/cm^3	0.0294 g/cm^3

The three density test samples were placed into a pycnometer to measure their volume shown in Table 12. The density of each sample, shown in Table 13, was calculated by dividing the mass of the sample in Table 5 by the volume in Table 12. In a study investigating cane sugar's physical and mechanical properties, the density at standard temperature and pressure (STP) is 1.59 g/cm³ [40]. The sample with a density closest to that was the first sample at 1.2873

g/cm³, 24% lower than the expected value from the study. A density value below the expected value could be attributed to the volume of the density test samples being less than 10% of the pycnometers sample chamber volume, as well as the samples having holes and irregularities. This leads to air entrapment, which means that air can become trapped within the sample which leads to an overestimation of the volume. As a result, the density will be underestimated, as shown in all three density tests.

Section 4.3: Geometry Shape Validation

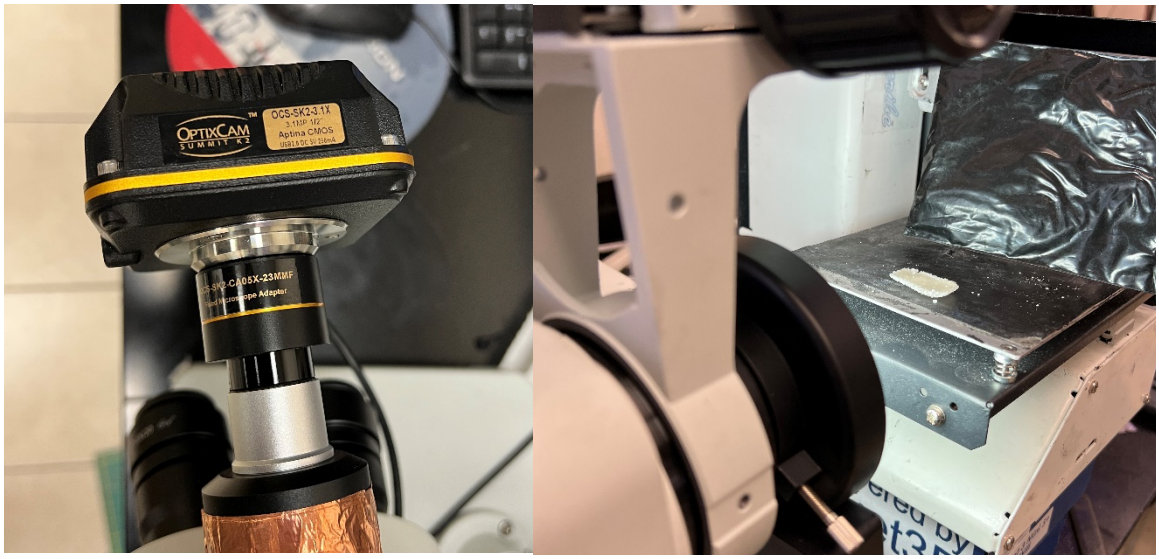


Figure 52: OptixCam Summit K2 Camera attached to Omano Microscope

This section reviews the geometry of one square and one density test sample through an OptixCam Summit K2 Camera attached to Omano Microscope. The OptixCam Summit K2 camera has a 16-megapixel sensor, which provides high-resolution images with excellent detail. It is connected through a USB 3.0 interface, which connects to software called ToupView on a computer. This camera is placed into an Omano microscope, allowing for the close-up images shown in Figure 53 and Figure 54.

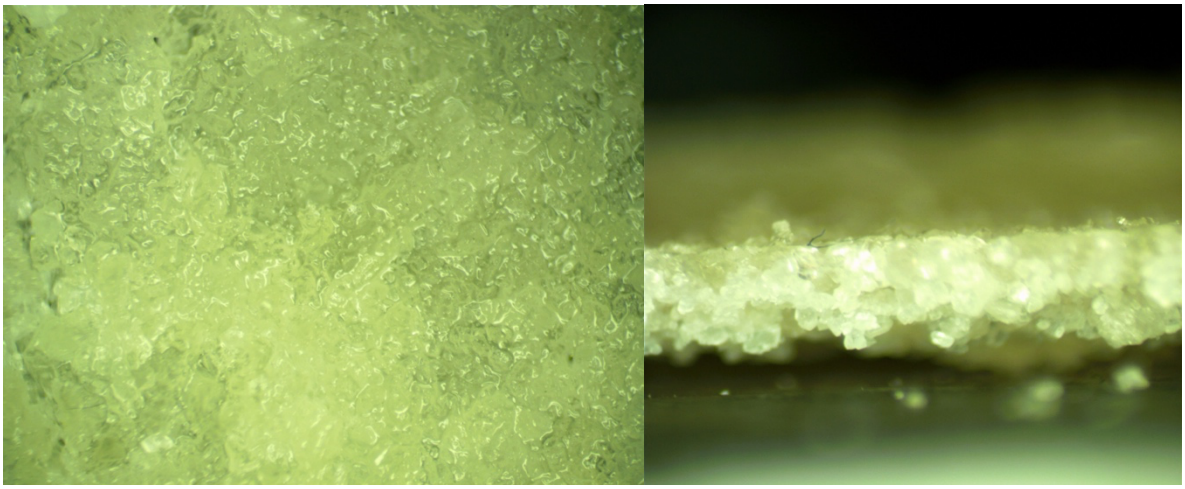


Figure 53: Close-up of the Sintered Sugar in a Square Sample

The pictures shown in Figure 53 are from the third square sample. The image on the left indicates that this sample has a smooth sintering profile with no gaps or holes. The sugar is bonded correctly, forming a strong and accurate structure. The image on the right also indicates the sample's relatively flat thickness profile. However, there was slight warping from the laser. Both images suggest that this printer can sinter correctly and accurately, which will help when starting to print in three dimensions in future research.

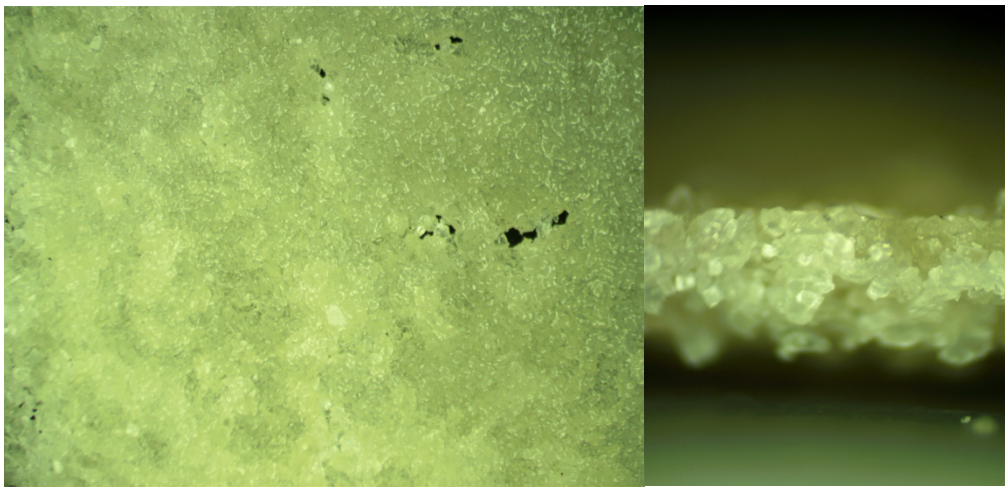


Figure 54: Close-up of the Sintered Sugar in a Density Test Sample

Unlike the pictures from the square sample, the density test sample has some holes and irregularities in the profile, as seen in Figure 54. As discussed in the previous section, air could be trapped within the holes, overestimating the volume, which resulted in an underestimation of the density. The holes in a sample after sintering could indicate insufficient heat during sintering. If the sample is not exposed to enough heat during the sintering process, it may not fully bond, leaving voids and holes in the sugar. Additionally, the cooling process after sintering should be carefully controlled to prevent dramatic drops in temperature, which could lead to cracking. Even though the profile has some holes, it is generally smooth and has a flat profile, as seen in the image on the right.

Chapter 5: Conclusion and Future Work

A large SLS 3D Printer was developed for additive sugar manufacturing for potential research in the biomedical field. The printer was designed to have a controllable heat chamber temperature, laser intensity, and laser scanning speed, as these parameters were the most important for correctly sintering sugar. It was also found that these three parameters were the key to eliminating holes or warping in sugar samples, as these allowed the sugar to sinter sufficiently. Various measurements and the geometry of single-layer sugar samples developed through selective laser sintering were studied.

Five different samples were designed in SolidWorks. Each sample was sliced using a custom configuration file in Slic3r, exported, and the G-Code was translated through a custom code to optimize it for this SLS 3D printer. The five samples included a square, density test, star, leaf, and bird. Each sample showcased unique complex sintering maneuvers necessary for potential biomedical applications. The printer can sinter sharp corners while maintaining a smooth infill. It also can sinter sugar around a center hole without bonding the sugar in the hole. The most impressive capability was being able to sinter in tight crevasses in the leaf and bird samples with such precision.

It was determined that the best printing parameters were a laser scanning speed of 0.5mm/s, laser intensity of 250, and a heat chamber temperature of 150℃. These parameters showed the best sample geometry and accuracy. The third square sample and third density test were the best simple single-layer samples. They had the best geometry because they were closest to the expected area. These samples were chosen to be evaluated under a microscope and showed little holes or warping, indicating proper sintering. They also exhibited flat thickness profiles which are necessary when starting to print in three dimensions.

Being able to print detailed geometries like the second bird sample shows that this printer can continue to be upgraded for more advanced biomedical engineering applications. Sugar skeletons, or saccharide scaffolds, are three-dimensional structures made from sugars. These skeletons are used as a template to assemble biologically active molecules or compounds [41]. They can also mimic the natural carbohydrates in living organisms and are used as probes to study cell-carbohydrate interactions and a scaffold for constructing new biologically active molecules [41]. This printer could also potentially help Dr. Yingtao Liu's research, where piezoelectric sensing devices were created by injecting electrically conductive nanocomposites into sacrificial sugar skeletons [9].

The work outlined in the thesis serves as a good basis for future improvements to the printer. The most important modification to the printer is fixing the sweeper arm to allow for an even deposition of sugar onto the fabrication piston, which will allow for three-dimensional printing. Once this is accomplished, three-dimensional samples can be produced and tested for real-world biomedical engineering applications.

References

[1] J. Giri, W. J. Li, R. S. Tuan, and M. T. Cicerone, "Stabilization of proteins by nanoencapsulation in sugar–glass for tissue engineering and drug delivery applications," *Advanced materials,* vol. 23, no. 42, pp. 4861-4867, 2011.

[2] J. Beaman, D. L. Bourell, C. Seepersad, and D. Kovar, "Additive manufacturing review: Early past to current practice," *Journal of Manufacturing Science and Engineering,* vol. 142, no. 11, 2020.

[3] K. V. Wong and A. Hernandez, "A review of additive manufacturing," *International scholarly research notices,* vol. 2012, 2012.

[4] M. Abshirini, M. Charara, P. Marashizadeh, M. C. Saha, M. C. Altan, and Y. Liu, "Functional nanocomposites for 3D printing of stretchable and wearable sensors," *Applied Nanoscience,* vol. 9, pp. 2071-2083, 2019.

[5] M. Abshirini, M. Charara, Y. Liu, M. Saha, and M. C. Altan, "3D printing of highly stretchable strain sensors based on carbon nanotube nanocomposites," *Advanced Engineering Materials,* vol. 20, no. 10, p. 1800425, 2018.

[6] B. Herren, M. C. Saha, M. C. Altan, and Y. Liu, "Development of ultrastretchable and skin attachable nanocomposites for human motion monitoring via embedded 3D printing," *Composites Part B: Engineering,* vol. 200, p. 108224, 2020.

[7] M. Abshirini, P. Marashizadeh, M. C. Saha, M. C. Altan, and Y. Liu, "Three-Dimensional Printed Highly Porous and Flexible Conductive Polymer Nanocomposites with Dual-Scale Porosity and Piezoresistive Sensing Functions," *ACS Applied Materials & Interfaces,* vol. 15, no. 11, pp. 14810-14825, 2023.

[8] M. Abshirini, M. C. Saha, M. C. Altan, and Y. Liu, "3D printed flexible microscaled porous conductive polymer nanocomposites for piezoresistive sensing applications," *Advanced Materials Technologies,* vol. 7, no. 9, p. 2101555, 2022.

[9] M. Charara, W. Luo, M. C. Saha, and Y. Liu, "Investigation of lightweight and flexible carbon nanofiber/poly dimethylsiloxane nanocomposite sponge for piezoresistive sensor application," *Advanced Engineering Materials,* vol. 21, no. 5, p. 1801068, 2019.

[10] L. A. Chavez *et al.*, "Fabrication and characterization of 3D printing induced orthotropic functional ceramics," *Smart Materials and Structures,* vol. 28, no. 12, p. 125007, 2019.

[11] L. A. Chavez *et al.*, "Electrical and mechanical tuning of 3D printed photopolymer–MWCNT nanocomposites through in situ dispersion," *Journal of Applied Polymer Science,* vol. 136, no. 22, p. 47600, 2019.

[12] M. Munsch, "Laser additive manufacturing of customized prosthetics and implants for biomedical applications," in *Laser additive manufacturing*: Elsevier, 2017, pp. 399-420.

[13] D. Radenkovic, A. Solouk, and A. Seifalian, "Personalized development of human organs using 3D printing technology," *Medical hypotheses,* vol. 87, pp. 30-33, 2016.

[14] C. Billings, C. Cai, and Y. Liu, "Utilization of antibacterial nanoparticles in photocurable additive manufacturing of advanced composites for improved public health," *Polymers,* vol. 13, no. 16, p. 2616, 2021.

[15] C. Billings, P. Kim, T. Shadid, J. D. Ballard, C. Cai, and Y. Liu, "Implementation of Antibacterial Nanoparticles in Additive Manufacturing to Increase Part Strength and Stiffness," *Journal of Composites Science,* vol. 6, no. 9, p. 248, 2022.

[16] M. R. de Campos, A. L. Botelho, and A. C. dos Reis, "Antimicrobial incorporation on 3D-printed polymers used as potential dental materials and biomaterials: A systematic review of the state of the art," *Polymer Bulletin,* pp. 1-28, 2022.
[17] K. Hölzl, S. Lin, L. Tytgat, S. Van Vlierberghe, L. Gu, and A. Ovsianikov, "Bioink properties before, during and after 3D bioprinting," *Biofabrication,* vol. 8, no. 3, p. 032002, 2016.
[18] S. Zhang and H. Wang, "Current progress in 3D bioprinting of tissue analogs," *SLAS TECHNOLOGY: Translating Life Sciences Innovation,* vol. 24, no. 1, pp. 70-78, 2019.
[19] I. Matai, G. Kaur, A. Seyedsalehi, A. McClinton, and C. T. Laurencin, "Progress in 3D bioprinting technology for tissue/organ regenerative engineering," *Biomaterials,* vol. 226, p. 119536, 2020.
[20] C. Mandrycky, Z. Wang, K. Kim, and D.-H. Kim, "3D bioprinting for engineering complex tissues," *Biotechnology advances,* vol. 34, no. 4, pp. 422-434, 2016.
[21] P. Prabhakaran *et al.*, "Prospect and retrospect of 3D bio-printing," *Acta Histochemica,* vol. 124, no. 7, p. 151932, 2022.
[22] K. H. C. Li *et al.*, "The role of 3D printing in anatomy education and surgical training: A narrative review," *MedEdPublish,* vol. 6, no. 2, 2017.
[23] P. A. Mills and D. K. Mills, "Reduced Supply in the Organ Donor Market and How 3D Printing Can Address This Shortage: A Critical Inquiry into the Collateral Effects of Driverless Cars," *Applied Sciences,* vol. 10, no. 18, p. 6400, 2020.
[24] C. Kryou, V. Leva, M. Chatzipetrou, and I. Zergioti, "Bioprinting for liver transplantation," *Bioengineering,* vol. 6, no. 4, p. 95, 2019.
[25] C. L. Ventola, "Medical applications for 3D printing: current and projected uses," *Pharmacy and Therapeutics,* vol. 39, no. 10, p. 704, 2014.
[26] S. Vanaei, M. Parizi, F. Salemizadehparizi, and H. Vanaei, "An overview on materials and techniques in 3D bioprinting toward biomedical application," *Engineered Regeneration,* vol. 2, pp. 1-18, 2021.
[27] F. Guillemot *et al.*, "Laser-assisted bioprinting to deal with tissue complexity in regenerative medicine," *Mrs Bulletin,* vol. 36, no. 12, pp. 1015-1019, 2011.
[28] P. Jain, H. Kathuria, and N. Dubey, "Advances in 3D bioprinting of tissues/organs for regenerative medicine and in-vitro models," *Biomaterials,* vol. 287, p. 121639, 2022.
[29] F. You, B. F. Eames, and X. Chen, "Application of extrusion-based hydrogel bioprinting for cartilage tissue engineering," *International journal of molecular sciences,* vol. 18, no. 7, p. 1597, 2017.
[30] I. T. Ozbolat and M. Hospodiuk, "Current advances and future perspectives in extrusion-based bioprinting," *Biomaterials,* vol. 76, pp. 321-343, 2016.
[31] F. Yu and D. Choudhury, "Microfluidic bioprinting for organ-on-a-chip models," *Drug discovery today,* vol. 24, no. 6, pp. 1248-1257, 2019.
[32] Ž. P. Kačarević *et al.*, "An introduction to 3D bioprinting: possibilities, challenges and future aspects," *Materials,* vol. 11, no. 11, p. 2199, 2018.
[33] S. Patra and V. Young, "A review of 3D printing techniques and the future in biofabrication of bioprinted tissue," *Cell biochemistry and biophysics,* vol. 74, pp. 93-98, 2016.
[34] I. Donderwinkel, J. C. Van Hest, and N. R. Cameron, "Bio-inks for 3D bioprinting: recent advances and future prospects," *Polymer Chemistry,* vol. 8, no. 31, pp. 4451-4471, 2017.

[35] B. Hoelzel, "Additive manufacturing of HDPE using selective laser sintering," 2019.
[36] W. Luo, M. Charara, M. C. Saha, and Y. Liu, "Fabrication and characterization of porous CNF/PDMS nanocomposites for sensing applications," *Applied Nanoscience,* vol. 9, pp. 1309-1317, 2019.
[37] I. Gibson and D. Shi, "Material properties and fabrication parameters in selective laser sintering process," *Rapid prototyping journal,* 1997.
[38] P. Rider, Ž. P. Kačarević, S. Alkildani, S. Retnasingh, R. Schnettler, and M. Barbeck, "Additive manufacturing for guided bone regeneration: A perspective for alveolar ridge augmentation," *International journal of molecular sciences,* vol. 19, no. 11, p. 3308, 2018.
[39] L. X. Yang, X. S. Yao, and Y. B. Xue, "Study on sucrose powder in selective laser sintering mechanism," in *Applied Mechanics and Materials*, 2014, vol. 541: Trans Tech Publ, pp. 209-213.
[40] S. Madhu, Y. Devarajan, and L. Natrayan, "Effective utilization of waste sugarcane bagasse filler-reinforced glass fibre epoxy composites on its mechanical properties-waste to sustainable production," *Biomass Conversion and Biorefinery,* pp. 1-8, 2023.
[41] E. Lenci, G. Menchi, and A. Trabocchi, "Carbohydrates in diversity-oriented synthesis: challenges and opportunities," *Organic & Biomolecular Chemistry,* vol. 14, no. 3, pp. 808-825, 2016.